Theoretical Formulation

6.1. Introduction

ARPS is a nonhydrostatic atmospheric prediction model and is appropriate for use on scales ranging from a few meters to hundreds of kilometers. It is based on compressible Navier-Stokes equations describing the atmospheric flow, and uses a generalized terrain-following coordinate system. A variety of physical processes are taken into account in the model system. In this chapter, we describe the theoretical and numerical formulation of the dynamic equations and the treatment of various physical processes.

In Section 6.2, the dynamic equations and their numerical formulations are first described. In Section 6.3, three closure schemes for subgrid-scale turbulence are discussed. In Section 6.4, several types of computational mixing are described, and in Section 6.5, various boundary condition options are presented. Sections 6.6, 6.7, and 6.8 describe, respectively, the treatment of microphysical processes, surface layer physics, and the soil model with coupled surface energy budget equations.

6.2. Dynamic Equations and Numerical Formulations

The governing equations of the atmospheric model component (as opposed to the other components of the model system such as the soil model) of the Advanced Regional Prediction System (ARPS) include momentum, heat (potential temperature), mass (pressure), water substances, turbulent kinetic energy (TKE), and the equation of state. These equations are represented in a curvilinear coordinate system which is orthogonal in the horizontal. The governing equations used are the result of direct transformation from the Cartesian system, and are expressed in a fully

conservative form. These equations are solved in a rectangular computational space. Solution algorithms are discussed in subsequent sections.

6.2.1. The coordinate system

The governing equations of ARPS are written in a curvilinear coordinate system (ξ, η, ζ) defined by

$$\begin{aligned} \xi &= x, \\ \eta &= y, \\ \zeta &= \zeta(x, y, z), \end{aligned} \tag{6.2.1}$$

or equivalently, by

$$\begin{aligned} x &= \xi, \\ y &= \eta, \\ z &= z(\xi, \eta, \zeta). \end{aligned} \tag{6.2.2}$$

This coordinate system is a special case of the fully three-dimensional curvilinear system, since the constant ξ and η surfaces remain the same as those of constant x and y. Vertical grid stretching and a lower grid surface that is conformal to the terrain are accommodated by the vertical transformation.

The governing equations for fluid motion in a fully 3-D curvilinear system can be found in the literature (*e.g.*, Thompson *et al.*, 1985). Sharman *et al*. (1988) and more recently Shyy and Vu (1991) discuss the choice of velocity vectors (covariant, contravariant and Cartesian velocity, *etc.*) that allow a conservative formulation of the momentum equations (see Appendix B). Following their work, we use the Cartesian velocity components instead of the contravariant components of velocity as the basic dependent variables.

As shown in Sharman *et al.* (1988), the Cartesian velocity components u, v and w can be expressed as functions of the contravariant velocities U^c, V^c and W^c,

$$\begin{aligned} u &= U^c \frac{\partial x}{\partial \xi} + V^c \frac{\partial x}{\partial \eta} + W^c \frac{\partial x}{\partial \zeta}, \\ v &= U^c \frac{\partial y}{\partial \xi} + V^c \frac{\partial y}{\partial \eta} + W^c \frac{\partial y}{\partial \zeta}, \\ w &= U^c \frac{\partial z}{\partial \xi} + V^c \frac{\partial z}{\partial \eta} + W^c \frac{\partial z}{\partial \zeta}. \end{aligned} \tag{6.2.3}$$

The inverse transformation is given by

$$
\begin{aligned}
U^c \sqrt{G} &= uJ^{yz}_{\eta\zeta} + vJ^{zx}_{\eta\zeta} + wJ^{xy}_{\eta\zeta} \,, \\
V^c \sqrt{G} &= uJ^{yz}_{\zeta\xi} + vJ^{zx}_{\zeta\xi} + wJ^{xy}_{\zeta\xi} \,, \\
W^c \sqrt{G} &= uJ^{yz}_{\xi\eta} + vJ^{zx}_{\xi\eta} + wJ^{xy}_{\xi\eta} \,,
\end{aligned}
\tag{6.2.4}
$$

where the Jacobians of transformation are defined as

$$
J^{yz}_{\eta\zeta} \equiv \frac{\partial(\,y,\,z\,)}{\partial(\,\eta,\,\zeta\,)} \quad , \tag{6.2.5}
$$

and $\sqrt{G}$ is the determinant of the Jacobian matrix of transformation from the (ξ, η, ζ) system to the (x, y, z) system:

$$
\sqrt{G} \equiv \frac{\partial(x,y,z)}{\partial(\xi,\eta,\zeta)} = \begin{vmatrix} x_\xi & x_\eta & x_\zeta \\ y_\xi & y_\eta & y_\zeta \\ z_\xi & z_\eta & z_\zeta \end{vmatrix} . \tag{6.2.6}
$$

A conservation equation in the transformed coordinate system for a scalar ϕ has the form

$$
\frac{\partial(\sqrt{G}\phi)}{\partial t} + \frac{\partial(\sqrt{G}U^c\phi)}{\partial\xi} + \frac{\partial(\sqrt{G}V^c\phi)}{\partial\eta} + \frac{\partial(\sqrt{G}W^c\phi)}{\partial\zeta} = S\sqrt{G} \,. \tag{6.2.7}
$$

assuming that the fluid is incompressible. In the above, S is a source and/or sink term for variable ϕ.

The coordinate transformations defined by (6.2.1) are

$$
\begin{aligned}
&J^{yz}_{\eta\zeta} \equiv \frac{\partial z}{\partial\zeta} \qquad J^{zx}_{\eta\zeta} \equiv 0 \qquad J^{xy}_{\eta\zeta} \equiv 0 \\
&J^{yz}_{\zeta\xi} \equiv 0 \qquad J^{zx}_{\zeta\xi} \equiv \frac{\partial z}{\partial\zeta} \qquad J^{xy}_{\zeta\xi} \equiv 0 \\
&J^{yz}_{\xi\eta} \equiv -\frac{\partial z}{\partial\xi} \quad J^{zx}_{\xi\eta} \equiv -\frac{\partial z}{\partial\eta} \quad J^{xy}_{\xi\eta} \equiv 1
\end{aligned}
\tag{6.2.8}
$$

and

$$\sqrt{G} = \left| \frac{\partial z}{\partial \zeta} \right|. \tag{6.2.9}$$

Note that most of these Jacobians are either zero or constant in this special case. We denote the non-zero components as

$$\begin{aligned} J_1 &\equiv J^{yz}_{\xi\eta} = - \frac{\partial z}{\partial \xi}, \\ J_2 &\equiv J^{zx}_{\xi\eta} = - \frac{\partial z}{\partial \eta}, \\ J_3 &\equiv J^{zx}_{\zeta\xi} = \frac{\partial z}{\partial \zeta}. \end{aligned} \tag{6.2.10}$$

The fully three dimensional transformation Jacobian $\sqrt{G}$ is thus

$$\sqrt{G} = | J_3 | . \tag{6.2.11}$$

According to the definition of the contravariant velocities in (6.2.4), we have

$$\begin{aligned} U^c &= u J_3 / \sqrt{G}, \\ V^c &= v J_3 / \sqrt{G}, \\ W^c &= (u J_1 + v J_2 + w) / \sqrt{G} \cdot \end{aligned} \tag{6.2.12}$$

Assuming that ζ increases monotonically with z, $J_3 \geq 0$ and therefore $J_3 = \sqrt{G}$. We also have $U^c = u$ and $V^c = v$. $J_3 \geq 0$ is always assumed in ARPS; therefore, J_3 is equivalent to $\sqrt{G}$ in the remainder of this Guide.

It follows that the transformation relations for spatial derivatives from Cartesian *(x,y,z)* coordinates to the curvilinear coordinate (ξ, η, ζ) are

$$\begin{aligned} \frac{\partial \phi}{\partial x} &= \frac{1}{\sqrt{G}} \left[\frac{\partial}{\partial \xi} (J_3 \phi) + \frac{\partial}{\partial \zeta} (J_1 \phi) \right] \\ \frac{\partial \phi}{\partial y} &= \frac{1}{\sqrt{G}} \left[\frac{\partial}{\partial \eta} (J_3 \phi) + \frac{\partial}{\partial \zeta} (J_2 \phi) \right] \\ \frac{\partial \phi}{\partial z} &= \frac{1}{\sqrt{G}} \frac{\partial \phi}{\partial \zeta}. \end{aligned} \tag{6.2.13}$$

In ARPS, the computational grid can be arbitrarily defined. The transformation Jacobians are calculated numerically according to (6.2.10) after the computational grid is defined. These Jacobians are used to formulate the governing equations in computational space. Section 7.3 discusses the available options for the computational grid setup in ARPS.

6.2.2. The governing equations

a) The model base state

In ARPS, wind components and the state variables are defined as the sums of base-state variables and the deviations from the base state. The base state is assumed to be horizontally homogeneous, time invariant and hydrostatically balanced. For this reason, the base-state mass and wind fields are, in general, not in a geostrophic balance, except when the base-state winds are zero.

In the model, the base state can be initialized using prescribed analytical functions or an external sounding. When the model is initialized using an external data set, the base state is usually constructed as the horizontal domain average. This is true when the external data set is created using ARPS external data pre-processor EXT2ARPS. *The horizontal homogeneity of the base state does not prevent one from initializing ARPS with fully 3-D initial fields. A base state that is closer to the total field will give better accuracy.*

The following model variables can be written as:

$$
\begin{aligned}
u\,(x,y,z,t) &= \bar{u}\,(z) + u'\,(x,y,z,t)\\
v\,(x,y,z,t) &= \bar{v}\,(z) + v'\,(x,y,z,t)\\
w\,(x,y,z,t) &= w'\,(x,y,z,t)\\
\theta\,(x,y,z,t) &= \bar{\theta}\,(z) + \theta'\,(x,y,z,t)\\
p\,(x,y,z,t) &= \bar{p}\,(z) + p'\,(x,y,z,t)\\
\rho\,(x,y,z,t) &= \bar{\rho}\,(z) + \rho'\,(x,y,z,t)\\
q_v\,(x,y,z,t) &= \bar{q}_v\,(z) + q_v'\,(x,y,z,t)\\
q_{li}\,(x,y,z,t) &= q_{li}'\,(x,y,z,t)
\end{aligned}
\qquad (6.2.14)
$$

where u, v and w are the Cartesian components of velocity (momentum), θ the potential temperature, p the pressure, ρ the density, q_v the water vapor mixing ratio, and q_{li} one of the hydrometeor categories. The over-barred variables

represent the base state and the primed variables are the deviations. The base state for w and q_{li} ' is assumed zero.

In the transformed coordinate system, Eqs. (6.2.14) become

$$\begin{aligned}
u(\xi,\eta,\zeta,t) &= \bar{u}(\xi,\eta,\zeta) + u'(\xi,\eta,\zeta,t) \\
v(\xi,\eta,\zeta,t) &= \bar{v}(\xi,\eta,\zeta) + v'(\xi,\eta,\zeta,t) \\
w(\xi,\eta,\zeta,t) &= w'(\xi,\eta,\zeta,t) \\
\theta(\xi,\eta,\zeta,t) &= \bar{\theta}(\xi,\eta,\zeta) + \theta'(\xi,\eta,\zeta,t) \\
p(\xi,\eta,\zeta,t) &= \bar{p}(\xi,\eta,\zeta) + p'(\xi,\eta,\zeta,t) \\
\rho(\xi,\eta,\zeta,t) &= \bar{\rho}(\xi,\eta,\zeta) + \rho'(\xi,\eta,\zeta,t) \\
q_v(\xi,\eta,\zeta,t) &= \bar{q}_v(\xi,\eta,\zeta) + q_{v'}(\xi,\eta,\zeta,t). \\
q_{li}(\xi,\eta,\zeta,t) &= q_{li}'(\xi,\eta,\zeta,t)
\end{aligned} \tag{6.2.15}$$

The original x- and y-independent base-state variables now become functions of all three independent variables (ξ, η, ζ) in the new coordinate system. Therefore, the base-state arrays in the model are three dimensional. The base-state arrays vary along the coordinate surfaces when these surfaces are not flat. This is usually true when terrain is included.

The base state atmosphere is assumed to satisfy the hydrostatic relation:

$$\frac{\partial \bar{p}}{\partial \zeta} = -\sqrt{G}\,\bar{\rho}\,g\,. \tag{6.2.16}$$

b) The governing equations

ARPS solves prognostic equations for u, v, w, θ', p' and q_ψ, which are, respectively, the x, y and z components of the Cartesian velocity, the perturbation potential temperature and perturbation pressure, and the six categories of water substance (water vapor, cloud water, rainwater, cloud ice, snow, and hail).

The equation of state for an atmosphere containing water constituents is given by (see Proctor, 1987)

$$\rho = \frac{p}{R_d T}\left(1 - \frac{q_v}{\varepsilon + q_v}\right)\left(1 + q_v + q_{liquid+ice\ water}\right) \tag{6.2.17}$$

where T is the air temperature, R_d the gas constant for dry air, and $\varepsilon \equiv R_d/R_v \approx 0.622$ is the ratio of the gas constants for dry air and water vapor. $q_{liquid\ +\ ice\ water}$ represents the total liquid and ice water content.

For convenience, we define the following variables:

$$\begin{aligned} \rho^* &= \sqrt{G}\,\bar{\rho} \\ u^* &= \rho^* u \\ v^* &= \rho^* v \\ w^* &= \rho^* w \\ W^{c*} &= \rho^* W^c. \end{aligned} \tag{6.2.18}$$

The momentum conservation equations are, respectively,

$$\begin{aligned} \frac{\partial u^*}{\partial t} = &- \left[u^* \frac{\partial u}{\partial \xi} + v^* \frac{\partial u}{\partial \eta} + W^{c*} \frac{\partial u}{\partial \zeta} \right] \\ &- \left[\frac{\partial}{\partial \xi} \left\{ J_3 (p' - \alpha Div^*) \right\} + \frac{\partial}{\partial \zeta} \left\{ J_1 (p' - \alpha Div^*) \right\} \right] \\ &+ \left[\rho^* f v - \rho^* \tilde{f} w \right] + \sqrt{G}\, D_u , \end{aligned} \tag{6.2.19}$$

$$\begin{aligned} \frac{\partial v^*}{\partial t} = &- \left[u^* \frac{\partial v}{\partial \xi} + v^* \frac{\partial v}{\partial \eta} + W^{c*} \frac{\partial v}{\partial \zeta} \right] \\ &- \left[\frac{\partial}{\partial \eta} \left\{ J_3 (p' - \alpha Div^*) \right\} + \frac{\partial}{\partial \zeta} \left\{ J_2 (p' - \alpha Div^*) \right\} \right] \\ &- \rho^* f u + \sqrt{G}\, D_v , \end{aligned} \tag{6.2.20}$$

$$\begin{aligned} \frac{\partial}{\partial t}(\rho^* w) = &- \left[u^* \frac{\partial w}{\partial \xi} + v^* \frac{\partial w}{\partial \eta} + W^{c*} \frac{\partial w}{\partial \zeta} \right] \\ &- \frac{\partial}{\partial \zeta} (p' - \alpha Div^*) + \rho^* B + \rho^* \tilde{f} u + \sqrt{G}\, D_w . \end{aligned} \tag{6.2.21}$$

Terms on the right hand side of Eqs. (6.2.19) and (6.2.20) are, in order, momentum advection, perturbation pressure gradient force and Coriolis force term. The terms D_u and D_v contain the subgrid scale turbulence and computational mixing terms. The Coriolis effect due to vertical motion is also included. The Coriolis coefficients are $f = 2\Omega \sin(\phi)$ and $\tilde{f} = 2\ \Omega \cos(\phi)$, where Ω is the angular velocity of the earth and ϕ is latitude. The horizontal base-state pressure gradient terms vanish because the base-state pressure is assumed to be horizontally homogeneous. The removal of the base-state pressure gradient terms from the equations reduces the computational error associated with the terrain-following coordinate (*e.g.*, Janjic, 1977).

In obtaining the above equations, *linearization approximations are made*. The state variables that appear in the coefficients of certain terms are replaced by their base-state values. This is true for the density in the pressure gradient force. These approximations are consistent with those in the anelastic systems (Ogura and Phillips, 1962; Wilhelmson and Ogura, 1972).

The vertical momentum equation (6.2.21) has one more term than horizontal momentum equations; the buoyancy term. The total buoyancy B is derived from the equation of state, (6.2.17):

$$B = -g\frac{\rho'}{\bar{\rho}} = g\left[\frac{\theta'}{\bar{\theta}} - \frac{p'}{\bar{\rho}c_s^2} + \frac{q'_v}{\varepsilon + \bar{q}_v} - \frac{q'_v + q_{liquid+ice}}{1 + \bar{q}_v}\right], \tag{6.2.22}$$

where $c_s \equiv \sqrt{\gamma R\bar{T}}$ is the acoustic wave speed, $\gamma \equiv C_p/C_v$ is the ratio of the specific heat of air at constant pressure and volume and R is the gas constant for dry air. Term $q_{liquid+ice}$ represents the total liquid and ice water content.

The terms involving $\alpha\ Div^*$ in Eqs. (6.2.19) — (6.2.21) are artificial "divergence damping" terms designed to attenuate acoustic waves, where Div^* is the density weighted divergence defined by

$$Div^* = \frac{1}{\sqrt{G}}\left[\frac{\partial u^*}{\partial \xi} + \frac{\partial v^*}{\partial \eta} + \frac{\partial W^{c*}}{\partial \zeta}\right], \tag{6.2.23}$$

and α is the damping coefficient.

The effect of these terms can be clearly seen by performing the divergence operation on the momentum equations, *i.e.*, *∂(6.2.19)/∂x + ∂(6.2.19)/∂y + ∂(6.2.19)/∂z* to obtain the following equation:

$$\frac{\partial}{\partial t}(Div^*) = \alpha \nabla^2 (Div^*) + ... \tag{6.2.24}$$

The divergence damping terms form a diffusion term acting on the three dimensional divergence, and thus serve to damp acoustic modes. Skamarock and Klemp (1992) show that unstable acoustic modes can be excited in the mode-splitting time integration system used by ARPS, but can be effectively controlled by divergence damping or by using backward-in-time biasing (Durran and Klemp, 1983) when the *w* and *p* equations are solved implicitly. The divergence damping has little effect on the meteorologically significant wave modes.

The mixing terms denoted by *D* in Eqs. (6.2.19)—(6.2.21) will be discussed separately in Section 6.3 and 6.4.

For thermal energy conservation, the potential temperature (θ) is the prognostic variable. The potential temperature is materially conservative in the absence of diabatic processes. In the model, the actual prognostic variable is the potential temperature perturbation, θ', and the associated equation is

$$\begin{aligned}\frac{\partial}{\partial t}(\rho^* \theta') = &-\left[u^* \frac{\partial \theta'}{\partial \xi} + v^* \frac{\partial \theta'}{\partial \eta} + W^{c*} \frac{\partial \theta'}{\partial \zeta}\right] \\ &-\left[\rho^* w \frac{\partial \bar{\theta}}{\partial z}\right] + \sqrt{G}\, D_\theta + \sqrt{G}\, S_\theta .\end{aligned} \tag{6.2.25}$$

The right hand side terms are, respectively, the perturbation potential temperature advection, the base-state potential temperature advection, mixing, and heat source / sink effects representing contributions from microphysical processes, radiation and any other heating / cooling effects. The horizontal advection of $\bar{\theta}$ vanishes because $\bar{\theta}$ is assumed to be horizontally homogeneous.

Among the three state variables (density, temperature and pressure), two should be predicted and the other diagnosed. Since the pressure is directly responsible for the mass balance in the system through the pressure gradient forces in the momentum equations, ARPS computes pressure. The pressure equation is obtained by taking the material derivative of the equation of state

and replacing the time derivative of density by velocity divergence using the continuity equation:

$$\begin{aligned}\frac{\partial}{\partial t}(J_3 p') = &- \left[(J_3 u)\frac{\partial p'}{\partial \xi} + (J_3 v)\frac{\partial p'}{\partial \eta} + (J_3 W^c)\frac{\partial p'}{\partial \zeta} \right] + J_3 \bar{\rho} g w \\ &- \bar{\rho} c_s^2 \left[\frac{\partial}{\partial \xi}(J_3 u) + \frac{\partial}{\partial \eta}(J_3 v) + \frac{\partial}{\partial \zeta}(J_3 W^c) \right] \\ &+ J_3 \bar{\rho} c_s^2 \left[\frac{1}{\theta}\frac{d\theta}{dt} - \frac{1}{E}\frac{dE}{dt} \right],\end{aligned} \tag{6.2.26}$$

where $E \equiv 1 + 0.61\, q_v + q_{liquid+ice}$.

The terms on the right hand side of Eq. (6.2.26) are the advection of perturbation pressure p', the advection of base-state pressure $\bar{p}$, the divergence term and the diabatic terms. The hydrostatic relation was used to substitute for the vertical gradient of $\bar{p}$ in the vertical $\bar{p}$ advection term. The divergence term is usually the dominant term for most meteorological applications. The diabatic terms are usually small, and are therefore neglected in ARPS. This same approximation was made in Klemp and Wilhelmson (1978).

The conservation equations for the mixing ratios of water vapor q_v, cloud water q_c, rainwater q_r, cloud ice q_i, snow q_s and hail q_h are written in a general form for a variable q_ψ as

$$\begin{aligned}\frac{\partial}{\partial t}(\rho^* q_\psi) = &- \left[u^* \frac{\partial q_\psi}{\partial \xi} + u^* \frac{\partial q_\psi}{\partial \eta} + W^{c*} \frac{\partial q_\psi}{\partial \zeta} \right] \\ &+ \frac{\partial(\rho^* V_{q_\psi} q_\psi)}{\partial \zeta} + \sqrt{G}\, D_{q_\psi} + \sqrt{G}\, S_{q_\psi}\end{aligned} \tag{6.2.27}$$

The right hand side terms are, in order, advection, sedimentation, mixing and source terms. The source term S_{q_ψ} represents all microphysical processes, which are discussed in Sections 6.6 and 6.7. The sedimentation term represents the falling of hydrometeors (rain, snow and hail) at their respective terminal speed. Cloud droplets and ice cloud are generally assumed to float with the air, therefore their flow-relative terminal velocity is zero.

6.2.3. The discretized form of the governing equations

a) The model grid

The continuous equations described in the previous section are solved numerically using finite difference methods on a rectangular computational grid. The model variables are staggered on an Arakawa C-grid, with scalars defined at the center of the grid boxes and the normal velocity components defined on the corresponding box faces. The coordinate variables *x*, *y* and *z* are also staggered and are defined at the *u*, *v* and *w* points, respectively. It follows that we should evaluate $J_1 = -\partial z/\partial \xi$ a half a grid interval below the u point, $J_2 = -\partial z/\partial \eta$ a half a grid interval below the v point, and $J_3 = \partial z/\partial \zeta$ and $\sqrt{G} = |J_3|$ at the scalar point. This spatial arrangement is illustrated in Figure 6.1.

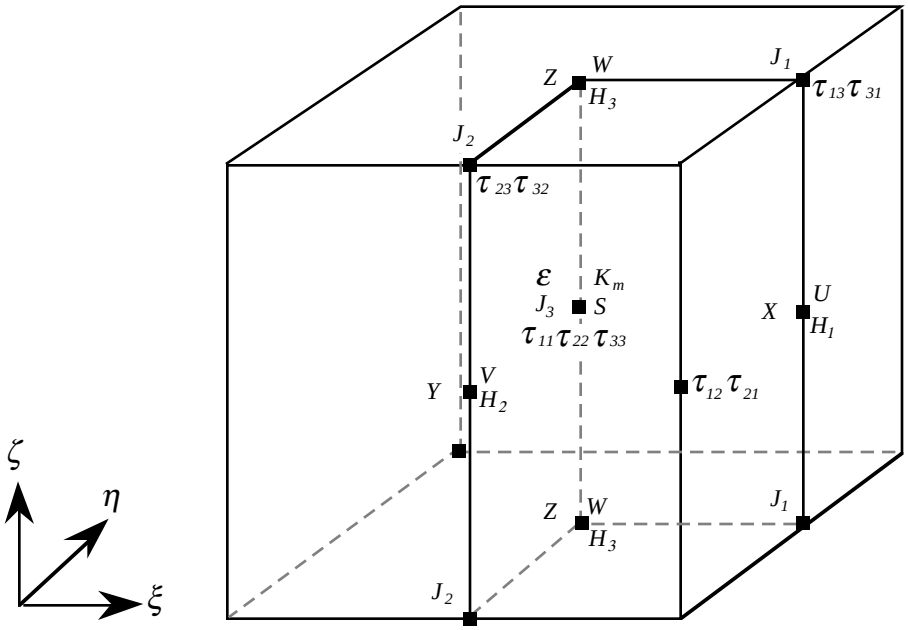

Figure 6.1. A grid box depicting the staggering of the coordinate and dependent variables.

To represent the governing equations in finite difference form, we define the following notations for averaging and differencing

$$\bar{\alpha}^{ns} = [\, \alpha(s + n\,\Delta s/2) + \alpha(s - n\Delta s/2)\,]/2$$

$$\delta_{ns}\alpha = [\, \alpha(s + n\,\Delta s/2) - \alpha(s - n\,\Delta s/2)\,]/(n\Delta s) \qquad (6.2.28)$$

where α is a dependent variable and *s* is an independent variable indicating the coordinate direction in which the operation takes place. *n* is an integer.

The numerical formulations of *u**, *v**, *w** and W^{c}* defined in (6.2.18) are:

$$\begin{aligned} u^* &= \overline{\rho^*}^{\xi} u, \\ v^* &= \overline{\rho^*}^{\eta} v, \\ w^* &= \overline{\rho^*}^{\zeta} w, \\ W^{c*} &= \overline{\rho^*}^{\zeta} W^{c}. \end{aligned} \tag{6.2.29}$$

The contravariant vertical velocity W^{c} is also defined at the *w* point, and is evaluated according to

$$W^{c} = \left(\overline{\overline{u^*}^{\zeta} J_1}^{\xi} + \overline{\overline{v^*}^{\zeta} J_2}^{\eta} + w^* \right) / \left(\overline{\sqrt{G}}^{\zeta} \overline{\rho^*}^{\zeta} \right). \tag{6.2.30}$$

Clark (1977) found that a proper discretization of this equation is very important in obtaining a correct kinetic energy budget in an anelastic model.

b) Numerical integration of governing equations

Since the model atmosphere described by the governing equations is compressible, meteorologically unimportant acoustic waves are also supported by the model. The presence of acoustic waves severely limits the time step size of explicit time integration schemes. To improve the model efficiency, the mode-splitting time integration technique presented in Klemp and Wilhelmson (1978) is employed. This technique divides a big integration time step into a number of computationally inexpensive small time steps and updates the acoustically active terms every small time step while computing all the other terms only once every big time step. Consequently, only the small time step size is limited by the acoustic wave speed.

The large time-step integration uses a centered three-level (leapfrog) time differencing scheme. With the exception of the advection terms, the spatial difference terms are second-order accurate. The advection, at the option of the user, can be either second- or fourth-order accurate. The large time interval is limited by a stability condition based on advective and (optionally) on gravity wave speeds. For the small time step integration, there

are two options. The first is the forward-backward scheme that is fully explicit. In this case, the momentum equations are first integrated one small time step using a forward scheme (relative to the pressure gradient force terms), then the pressure equation is integrated forward using a backward scheme (relative to the divergence term which uses the updated velocities). The other option is the Crank-Nicolson scheme which solves the *w* and *p* equations implicitly in the vertical direction. The algorithm is absolutely stable with respect to vertical acoustic waves. The small time step size is, in this case, independent of the vertical grid spacing, therefore allowing a much larger time step size when the horizontal to vertical grid aspect ratio is large. An implicit step is more expensive than an explicit step due to the need to solve a tridiagonal system at each time step.

ARPS also provides an option for including the gravity wave modes in the small time steps. This involves evaluating the thermal buoyancy and base state potential temperature advection term on the small time step, and stepping the θ equation there as well.

The finite difference form of the *u, v, w, p* and θ equations are:

$$\overline{\rho^*}^{\xi} \frac{u^{\tau+\Delta\tau} - u^{\tau}}{\Delta\tau} =$$

$$- \left[\delta_{\xi}\left\{ J_3 \, (p' - \alpha \, Div^*) \right\} + \delta_{\zeta}\left\{ J_1 \, \overline{p' - \alpha \, Div^*}^{\,\zeta\xi} \right\} \right]^{\tau} + f_u^t \,, \qquad (6.2.31a)$$

$$\overline{\rho^*}^{\eta} \frac{v^{\tau+\Delta\tau} - v^{\tau}}{\Delta\tau} =$$

$$- \left[\delta_{\eta}\left\{ J_3 \, (p' - \alpha \, Div^*) \right\} + \delta_{\zeta}\left\{ J_2 \, \overline{p' - \alpha \, Div^*}^{\,\zeta\eta} \right\} \right]^{\tau} + f_v^t \,, \qquad (6.2.31b)$$

$$\overline{\rho^*}^{\zeta} \frac{w^{\tau+\Delta\tau} - w^{\tau}}{\Delta\tau} =$$

$$+ \alpha \left[\delta_{\zeta} Div^* \right]^{\tau} + \left[\overline{g \, \rho^* \, \theta' / \bar{\theta}}^{\,\zeta} \right]^{\tau} - \left[\beta \, \delta_{\zeta} p'^{\tau+\Delta\tau} + (1-\beta) \, \delta_{\zeta} p'^{\tau} \right]$$

$$- \left[\beta \left\{ \overline{g J_3 \, p' / c_s^2}^{\,\zeta} \right\}^{\tau+\Delta\tau} + (1-\beta) \left\{ \overline{g J_3 \, p' / c_s^2}^{\,\zeta} \right\}^{\tau} \right] + f_w^t \,, \qquad (6.2.31c)$$

$$
\begin{aligned}
J_3 \frac{p'^{\tau+\Delta\tau} - p'^{\tau}}{\Delta\tau} \; = \; & \\
& - \bar{\rho}\, c_s^2 \left[\delta_\xi(\bar{J}_3^{\,\xi} u) + \delta_\zeta(\overline{J_1 \bar{u}^{\zeta}}^{\xi}) + \delta_\eta (\bar{J}_3^{\,\eta} v) + \delta_\zeta(\overline{J_2 \bar{v}^{\zeta}}^{\eta}) \right]^{\tau+\Delta\tau} \\
& - \bar{\rho}\, c_s^2 \left[\beta\, \delta_\zeta w^{\tau+\Delta\tau} + (1-\beta)\, \delta_\zeta w^{\tau} \right] \\
& + g\rho^* \left[\beta \left(\bar{w}^{\zeta} \right)^{\tau+\Delta\tau} + (1-\beta) \left(\bar{w}^{\zeta} \right)^{\tau} \right] + f_p^{\,t} \,,
\end{aligned}
\tag{6.2.31d}
$$

$$
\rho^* \frac{\theta'^{\tau+\Delta\tau} - \theta'^{\tau}}{\Delta\tau} = - \left[\overline{\bar{\rho}^{\zeta} w\, \delta_\zeta \bar{\theta}^{\zeta}}^{\tau} \right] + f_\theta^t \,. \tag{6.2.31e}
$$

The acoustically active terms include the pressure gradient force, divergence damping, divergence term in the pressure equation, buoyancy due to pressure perturbation (related to compressibility) and vertical pressure advection. The terms responsible for internal gravity waves include the buoyancy due to temperature perturbations and the vertical advection of the base-state potential temperature. The terms that are not responsible for acoustic or gravity wave modes are contained in f^t.

For each big time step, the u, v, w, p' and θ' equations are integrated forward from t-Δt and t+Δt during n_s number of small time steps, where Δt is the big time step size. The small time step size, $\Delta\tau$, satisfies equation $2\Delta t = n_s \Delta\tau$. The superscripts t and τ in (6.2.31) indicate the time level at which the terms are evaluated. The terms with superscript τ or $\tau+\Delta\tau$ are evaluated every small time step and those with superscript t are evaluated once every big time step and kept fixed throughout the small steps.

In Eqs. (6.2.31c) and (6.2.31d), time averaging is performed on several terms with β as the weighting coefficient. For the vertically explicit option, β is set to zero in the w equation and to unity in the p equation. In this case, the u, v and w equations are stepped forward one time step, then the p equation is integrated forward using the updated u, v and w. Relative to the divergence term, the time integration for pressure is backward. For $\beta \neq 0$, the time integration for the w and p equations becomes implicit. For $\beta = 0.5$, the averaging is centered in time and equivalent to that used by Klemp and Wilhelmson (1978).

Skamarock and Klemp (1993) showed that the mode-splitting scheme used here is unstable to certain acoustic waves due to the interaction between the advection and propagation of these waves. Durran and Klemp (1983) found that a value of β between 0.5 and 1.0 (effectively biasing the scheme towards backward-in-time) can damp certain unstable acoustic modes in a compressible model. Ikawa (1988) showed that, for β = 1, the scheme is neutral to horizontally propagating acoustic waves but severely damps the vertical modes. In general, a value of 0.6 is sufficient to control unstable acoustic modes.

Divergence damping is another effective way of controlling the unstable modes, and is the only method available for the explicit option. Finally, with the unstable modes effectively under control, the vertically implicit scheme is absolutely stable to vertically propagating acoustic waves. The solution procedure for the implicit option is given in the next subsection.

It should be noted that, in (6.2.31), we include the buoyancy due to pressure perturbation $[gp'/(\bar{\rho}c^2)]$ and the vertical base-state pressure advection $[-\rho gw]$ inside the small time steps. These two terms are found to be responsible for certain high frequency oscillations, and must be treated in this manner.

c) Terms not related to acoustic or gravity waves

The remaining non-acoustic and non-gravity wave terms in the governing equations are:

$$f_u^t = -ADVU^t + \left[\overline{\overline{\rho^* f \bar{v}^{\eta}}^{\xi}} - \overline{\overline{\rho^* \tilde{f} \bar{w}^{\zeta}}^{\xi}} \right]^t + J_3 D_u^{t-\Delta t}, \tag{6.2.32a}$$

$$f_v^t = -ADVV^t - \left[\overline{\overline{\rho^* f \bar{u}^{\xi}}^{\eta}} \right]^t + J_3 D_v^{t-\Delta t}, \tag{6.2.32b}$$

$$f_w^t = -ADVW^t + \left[\overline{\overline{\rho^* B_q}^{\zeta}} \right]^t + \left[\overline{\overline{\rho^* \tilde{f} \bar{u}^{\xi}}^{\zeta}} \right]^t + J_3 D_w^{t-\Delta t}, \tag{6.2.32c}$$

$$f_p^t = -ADVP^t, \tag{6.2.32d}$$

$$f_\theta^t = -ADVT^t + J_3 D_\theta^{t-\Delta t} + J_3 S_\theta^t, \tag{6.2.32e}$$

where B_q, the water substance contribution to buoyancy, is defined by Eq.(6.2.36) and *ADVU, ADVV, ADVW, ADVP* and *ADVT* are the advection terms for *u, v, w, θ'* and *p'*, respectively. The discrete formulations for them depend on the choice of advection schemes. ARPS 4.0 has options for second and fourth order centered differencing. The second-order advection terms are given by

$$ADVU = \overline{\overline{u^*}^{\xi}\delta_\xi u}^{\xi} + \overline{\overline{v^*}^{\xi}\delta_\eta u}^{\eta} + \overline{\overline{W^{c*}}^{\xi}\delta_\zeta u}^{\zeta},$$

$$ADVV = \overline{\overline{u^*}^{\eta}\delta_\xi v}^{\xi} + \overline{\overline{v^*}^{\eta}\delta_\eta v}^{\eta} + \overline{\overline{W^{c*}}^{\eta}\delta_\zeta v}^{\zeta},$$

$$ADVW = \overline{\overline{u^*}^{\zeta}\delta_\xi w}^{\xi} + \overline{\overline{v^*}^{\zeta}\delta_\eta w}^{\eta} + \overline{\overline{W^{c*}}^{\zeta}\delta_\zeta w}^{\zeta},$$

$$ADVP = \overline{\overline{J_3}^{\xi} u\,\delta_\xi p'}^{\xi} + \overline{\overline{J_3}^{\eta} v\,\delta_\eta p'}^{\eta} + \overline{\overline{J_3}^{\zeta} W^c\,\delta_\zeta p'}^{\zeta},$$

$$ADVT = \overline{u^*\,\delta_\xi \theta'}^{\xi} + \overline{v^*\,\delta_\eta \theta'}^{\eta} + \overline{W^{c*}\,\delta_\zeta \theta'}^{\zeta}. \qquad (6.2.33)$$

The fourth-order terms can be expressed as a weighted average of two terms:

$$ADVU = \frac{4}{3}\left[\overline{\overline{u^*}^{\xi}\delta_\xi u}^{\xi} + \overline{\overline{v^*}^{\xi}\delta_\eta u}^{\eta} + \overline{\overline{W^{c*}}^{\xi}\delta_\zeta u}^{\zeta}\right] - \frac{1}{3}\left[\overline{\overline{u^*}^{2\xi}\delta_{2\xi} u}^{2\xi} + \overline{\overline{v^*}^{\xi\eta}\delta_{2\eta} u}^{2\eta} + \overline{\overline{W^{c*}}^{\xi\zeta}\delta_{2\zeta} u}^{2\zeta}\right],$$

$$ADVV = \frac{4}{3}\left[\overline{\overline{u^*}^{\eta}\delta_\xi v}^{\xi} + \overline{\overline{v^*}^{\eta}\delta_\eta v}^{\eta} + \overline{\overline{W^{c*}}^{\eta}\delta_\zeta v}^{\zeta}\right] - \frac{1}{3}\left[\overline{\overline{u^*}^{\eta\xi}\delta_{2\xi} v}^{2\xi} + \overline{\overline{v^*}^{2\eta}\delta_{2\eta} v}^{2\eta} + \overline{\overline{W^{c*}}^{\eta\zeta}\delta_{2\zeta} v}^{2\zeta}\right],$$

$$ADVW = \frac{4}{3}\left[\overline{\overline{u^*}^{\zeta}\delta_\xi w}^{\xi} + \overline{\overline{v^*}^{\zeta}\delta_\eta w}^{\eta} + \overline{\overline{W^{c*}}^{\zeta}\delta_\zeta w}^{\zeta}\right] - \frac{1}{3}\left[\overline{\overline{u^*}^{\zeta\xi}\delta_{2\xi} w}^{2\xi} + \overline{\overline{v^*}^{\zeta\eta}\delta_{2\eta} w}^{2\eta} + \overline{\overline{W^{c*}}^{2\zeta}\delta_{2\zeta} w}^{2\zeta}\right],$$

$$
\begin{aligned}
ADVP = & \frac{4}{3}\left[\overline{\overline{J_3}^{\xi} u\, \delta_{\xi} p'}^{\xi} + \overline{\overline{J_3}^{\eta} v\, \delta_{\eta} p'}^{\eta} + \overline{\overline{J_3}^{\zeta} W^{c}\ \delta_{\zeta} p'}^{\zeta} \right] \\
& - \frac{1}{3}\left[\overline{\overline{\overline{J_3}^{\xi} u}^{\xi}\ \delta_{2\xi} p'}^{2\xi} + \overline{\overline{\overline{J_3}^{\eta} v}^{\eta}\ \delta_{2\eta} p'}^{2\eta} + \overline{\overline{\overline{J_3}^{\zeta} W^{c}}^{\zeta}\ \delta_{2\zeta} p'}^{2\zeta} \right], \\
ADVT = & \frac{4}{3}\left[\overline{u^{*}\, \delta_{\xi}\theta'}^{\xi} + \overline{v^{*}\, \delta_{\eta}\theta'}^{\eta} + \overline{W^{c*}\, \delta_{\zeta}\theta'}^{\zeta} \right] \\
& - \frac{1}{3}\left[\overline{\overline{u^{*}}^{\xi}\, \delta_{2\xi}\theta'}^{2\xi} + \overline{\overline{v^{*}}^{\eta}\, \delta_{2\eta}\theta'}^{2\eta} + \overline{\overline{W^{c*}}^{\zeta}\, \delta_{2\zeta}\theta'}^{2\zeta} \right].
\end{aligned}
\tag{6.2.34}
$$

It can be shown (Xue and Lin, 1991, unpublished manuscript) that these terms are fourth order for constant flows. When the flow is not constant, the truncation error is proportional to the gradient in the velocity field, and the error is smaller than that of the fourth order scheme presented by Wilhelmson and Chen (1983).

The above advection terms are written in advective form. Xue and Lin (1991) showed that this form is numerically equivalent to the flux form consisting of a flux term plus an anelastic correction that is often used by other modelers (*e.g.*, Wilhelmson and Chen, 1983). For example, consider the second order advection for potential temperature. We have

$$
\begin{aligned}
& \overline{u^{*}\, \delta_{\xi}\theta'}^{\xi} + \overline{v^{*}\, \delta_{\eta}\theta'}^{\eta} + \overline{W^{c*}\, \delta_{\zeta}\theta'}^{\zeta} \\
& \quad \equiv \delta_{\xi}(u^{*}\, \overline{\theta'}^{\xi}) + \delta_{\eta}(v^{*}\, \overline{\theta'}^{\eta}) + \delta_{\eta}(W^{c*}\, \overline{\theta'}^{\eta}) + \theta'\, Div^{*} .
\end{aligned}
\tag{6.2.35}
$$

In an anelastic system, *Div** = 0 and thus the advection can be written in a conservative flux form. In a compressible system, *Div** is not completely negligible but should remain small (it is actually damped by the divergence damping). Neglecting the effect of compressibility, both the second order and fourth order advection formulations given above are quadratically conservative (Xue and Lin, 1991; Arakawa and Lamb, 1977).

Term B_q in Eq.(6.2.32c) is the contribution to the buoyancy by water substance and is given by

$$
B_q = g\left[\frac{q_v'}{\varepsilon + \bar{q}_v} - \frac{q_v' + q_{liquid+ice}}{1 + \bar{q}_v} \right]. \tag{6.2.36}
$$

The advection, Coriolis force and B_q are evaluated at the current time level of the leapfrog integration. The turbulence and computational mixing terms are, however, evaluated, due to stability requirement, at the previous time level.

It should also be noted that the discretized Coriolis terms satisfy the conservation of energy implied by their continuous form.

The equations for water substances are solved completely on the big time step, and the numerical formulation is given in a general form for q_ψ as

$$\rho^* \frac{q_\psi^{t+\Delta t} - q_\psi^{t-\Delta t}}{2\Delta t} = -ADVQ^t + J_3 D_{q_\psi}^{t-\Delta t} + J_3 S_{q_\psi}^t \tag{6.2.37}$$

where the advection term *ADVQ* is given by the second order advection scheme

$$ADVQ = \overline{u^* \delta_\xi q_\psi}^{\xi} + \overline{v^* \delta_\eta q_\psi}^{\eta} + \overline{W^{c*} \delta_\zeta q_\psi}^{\zeta} \tag{6.2.38}$$

or by the fourth order advection scheme

$$\begin{aligned} ADVQ = & \frac{4}{3}\left[\overline{u^* \delta_\xi q_\psi}^{\xi} + \overline{v^* \delta_\eta q_\psi}^{\eta} + \overline{W^{c*} \delta_\zeta q_\psi}^{\zeta} \right] \\ & - \frac{1}{3}\left[\overline{\overline{u^{*\xi}} \delta_{2\xi} q_\psi}^{2\xi} + \overline{\overline{v^{*\eta}} \delta_{2\eta} q_\psi}^{2\eta} + \overline{\overline{W^{c*}}^{\zeta} \delta_{2\zeta} q_\psi}^{2\zeta} \right]. \end{aligned} \tag{6.2.39}$$

Again, the advection is calculated at the center time level (t) of the leapfrog time step and the mixing terms at the past time level (t-Δt).

c) The vertically implicit pressure and w solver

When the time averaging coefficient β is not zero, Eqs. (6.2.31c) and (6.2.31d) become simultaneous equations for w and p' at future time step. These two equations have to be solved together.

After regrouping the unknown terms, the pressure equation (6.2.31d) can be rewritten as

$$p'^{\tau+\Delta\tau} = p'^{\tau} + F_p + \frac{\Delta\tau}{J_3}\beta\left[\, g\rho^* \bar{w}^{\zeta} - \bar{\rho}\, c_s^2 \delta_\zeta w \,\right]^{\tau+\Delta\tau} \tag{6.2.40}$$

where

$$F_p = \frac{\Delta\tau}{J_3}\Big(f_p{}^t + (1-\beta)\left[\, g\rho^* \bar{w}^{\zeta} - \bar{\rho}\, c_s^2 \delta_\zeta w \,\right]^{\tau}\Big) - \frac{\Delta\tau}{J_3}\,\bar{\rho}\, c_s^2 \left[\delta_\xi(\overline{J_3}^{\xi} u) + \delta_\zeta(\overline{J_1 \bar{u}^{\zeta}}^{\xi}) + \delta_\eta(\overline{J_3}^{\eta} v) + \delta_\zeta(\overline{J_2 \bar{v}^{\zeta}}^{\eta})\,\right]^{\tau+\Delta\tau}. \tag{6.2.41}$$

On the right hand side of (6.2.40), only the third term involving w at $\tau+\Delta\tau$ is unknown.

Eliminating $p'^{\tau+\Delta\tau}$ in w equation (6.2.31c) using (6.2.40) yields

$$w^{\tau+\Delta\tau} = w^{\tau} + F_w - \frac{\Delta\tau^2\beta^2}{\overline{\rho^*}^{\zeta}}\,\delta_\zeta\left[\frac{g\,\rho^*}{J_3}\,\bar{w}^{\zeta} - \frac{\bar{\rho}\, c_s^2}{J_3}\,\delta_\zeta w\right]^{\tau+\Delta\tau} - \frac{\Delta\tau^2\beta^2 g}{\overline{\rho^*}^{\zeta}}\left[\frac{\overline{g\,\rho^*}^{\zeta}}{c_s^2}\,\bar{w}^{\zeta} - \overline{\bar{\rho}\,\delta_\zeta w}^{\zeta}\right]^{\tau+\Delta\tau} \tag{6.2.42}$$

where the known terms on the right hand side are grouped into F_w as

$$F_w = \frac{\Delta\tau}{\overline{\rho^*}^{\zeta}}\left\{ f_w^t - \delta_\zeta\left(p'^{\tau} - \alpha\, Div^*\right)^{\tau} + \left[\overline{g\,\rho^*\left(\frac{\theta'}{\bar{\theta}} - \frac{p'}{\bar{\rho} c_s^2}\right)}^{\zeta}\right]^{\tau} - \beta\,\overline{\left(g J_3\, F_p / c_s^2\right)}^{\zeta} - \beta\,\delta_\zeta F_p \right\}. \tag{6.2.43}$$

Note that ARPS has the option of calculating the thermal buoyancy term on the large time step.

Eq. (6.2.42) now has only one unknown, $w^{\tau+\Delta\tau}$, and the spatial averaging and differencing are all performed in the vertical direction. This equation is discretized using the second order scheme. After considerable algebra, we arrive at the following equation:

$$A_k\, w_{k-1} + B_k\, w_k + C_k\, w_{k+1} = D_k\,, \tag{6.2.44}$$

where

$$A_k = (- N_k c_s^2{}_{k-1} + P_k J_{3\,k-1}) (M_{k-1} + L_{k-1}) ,$$

$$B_k = 1 + N_k [(M_k + L_k) c^2{}_k - (M_{k-1} - L_{k-1}) c_s^2{}_{k-1}] + P_k [(M_k + L_k) J_{3\,k} + (M_{k-1} - L_{k-1}) J_{3\,k-1} ,$$

$$C_k = (N_k c_s^2{}_k + P_k J_{3\,k}) (M_k - L_k) ,$$

$$D_k = F_{w\,k} + w\tau_k , \qquad (6.2.45)$$

with $$P_k = \frac{\Delta\tau^2\beta^2 g}{2\,\overline{\rho^*}^{\zeta}}, \quad N_k = \frac{\Delta\tau^2\beta^2}{\Delta\zeta\,\overline{\rho^*}^{\zeta}}, \quad M_k = \frac{g\,\rho^*}{2\,J_3 c_s^2}, \quad L_k = \frac{\rho^*}{\Delta\zeta\,J_3^2} .$$

Equation (6.2.44) forms a linear tridiagonal equation system, and can be solved using a standard tridiagonal solver given appropriate boundary conditions. The same equation system also appears in the Poisson equation solver using alternating direction implicit (ADI) method described in Section 9.3. The procedure described there is used to solve (6.2.44).

In ARPS, only non-penetrative top and boundary conditions are supported by the vertically implicit solver. In this case, w at the top boundary (w_{nz-1}) is set to zero, and w at the lower boundary (w_2) is calculated from the horizontal velocities and the terrain height, ensuring that the flow at the lower boundary follows the terrain. The top and bottom boundary conditions are discussed further in Section 6.5.

After $w^{\tau+\Delta\tau}$ is solved from (6.2.44), it is substituted into Eq. (6.2.40) to yield pressure $p'^{\tau+\Delta\tau}$.

6.3. Subgrid Scale Turbulence Closure

6.3.1. Introduction

Turbulence parameterization, the closure linking the resolved scales and the unresolved subgrid-scale (SGS), is critical to the successful simulation of many flows. This section discusses three available options in ARPS for parameterizing the subgrid scale turbulence - the Smagorisky, 1.5 order turbulent kinetic energy (TKE) and Germano dynamic subgrid-scale (SGS) closure schemes. The Smagorinsky scheme is a special case of the TKE equation. The Germano dynamic SGS closure converts previously prescribed SGS model coefficients to self-determined parameters that vary with time and

space. In version 4.0 of ARPS, the Germano scheme is only available for the flat-terrain formulation.

6.3.2. The turbulent mixing formulations

The turbulent mixing terms in the governing equations (6.2.19) — (6.2.21), (6.2.25) and (6.2.27) are described in detail in this section. For the momentum equations, these terms are expressed in terms of the Reynolds stress tensor τ_{ij}, as

$$\begin{aligned}
\sqrt{G}\, D_u &= \sqrt{G}\left(\frac{\partial \tau_{11}}{\partial x} + \frac{\partial \tau_{12}}{\partial y} + \frac{\partial \tau_{13}}{\partial z} \right) \\
&= \frac{\partial}{\partial \xi}\left(J_3\, \tau_{11} \right) + \frac{\partial}{\partial \eta}\left(J_3\, \tau_{12} \right) + \frac{\partial}{\partial \zeta}\left(\tau_{13} + J_1\, \tau_{11} + J_2\, \tau_{12} \right), \\
\sqrt{G}\, D_v &= \sqrt{G}\left(\frac{\partial \tau_{21}}{\partial x} + \frac{\partial \tau_{22}}{\partial y} + \frac{\partial \tau_{23}}{\partial z} \right) \\
&= \frac{\partial}{\partial \xi}\left(J_3\, \tau_{21} \right) + \frac{\partial}{\partial \eta}\left(J_3\, \tau_{22} \right) + \frac{\partial}{\partial \zeta}\left(\tau_{23} + J_1\, \tau_{21} + J_2\, \tau_{22} \right), \\
\sqrt{G}\, D_w &= \sqrt{G}\left(\frac{\partial \tau_{31}}{\partial x} + \frac{\partial \tau_{32}}{\partial y} + \frac{\partial \tau_{33}}{\partial z} \right) \\
&= \frac{\partial}{\partial \xi}\left(J_3\, \tau_{31} \right) + \frac{\partial}{\partial \eta}\left(J_3\, \tau_{32} \right) + \frac{\partial}{\partial \zeta}\left(\tau_{33} + J_1\, \tau_{31} + J_2\, \tau_{32} \right).
\end{aligned} \tag{6.3.1}$$

The stress tensor is parameterized in terms of the resolvable scale quantities:

$$
\begin{aligned}
\tau_{11} &= \bar{\rho} K_{mh} (D_{11} - \frac{2}{3} Div) , \\
\tau_{12} &= \bar{\rho} K_{mh} D_{12} , \\
\tau_{13} &= \bar{\rho} K_{mv} D_{13} , \\
\tau_{21} &= \bar{\rho} K_{mh} D_{12} , \\
\tau_{22} &= \bar{\rho} K_{mh} (D_{22} - \frac{2}{3} Div) , \\
\tau_{23} &= \bar{\rho} K_{mv} D_{23} , \\
\tau_{31} &= \bar{\rho} K_{mh} D_{13} , \\
\tau_{32} &= \bar{\rho} K_{mh} D_{23} , \\
\tau_{33} &= \bar{\rho} K_{mh} (D_{33} - \frac{2}{3} Div) .
\end{aligned}
\tag{6.3.2}
$$

Here K_{mh} and K_{mv} are horizontal and vertical turbulent mixing coefficients for momentum. We distinguish the horizontal value from the vertical to make provision for considering anisotropic turbulence. D_{ij} is the deformation tensor, and *Div*, the velocity divergence, is defined as

$$
Div = \frac{1}{\sqrt{G}} \left(\frac{\partial(\sqrt{G} u)}{\partial \xi} + \frac{\partial(\sqrt{G} v)}{\partial \eta} + \frac{\partial(\sqrt{G} W^c)}{\partial \zeta} \right) . \tag{6.3.3}
$$

With respect to the stress tensor, the divergence terms are small and therefore are neglected in ARPS.

The deformation tensor, D_{ij} in (6.3.2), is given by

$$
\begin{aligned}
D_{11} &= 2 \frac{\partial u}{\partial x} = \frac{2}{\sqrt{G}} \left[\frac{\partial(J_3 u)}{\partial \xi} + \frac{\partial(J_1 u)}{\partial \zeta} \right], \\
D_{22} &= 2 \frac{\partial v}{\partial y} = \frac{2}{\sqrt{G}} \left[\frac{\partial(J_3 v)}{\partial \eta} + \frac{\partial(J_2 v)}{\partial \zeta} \right], \\
D_{33} &= 2 \frac{\partial w}{\partial z} = \frac{2}{\sqrt{G}} \frac{\partial w}{\partial \zeta} , \\
D_{12} &= \frac{\partial u}{\partial y} + \frac{\partial v}{\partial x} = \frac{1}{\sqrt{G}} \left[\frac{\partial}{\partial \eta}(J_3 u) + \frac{\partial}{\partial \xi}(J_3 v) + \frac{\partial}{\partial \zeta} (J_2 u + J_1 v) \right],
\end{aligned}
\tag{6.3.4}
$$

$$D_{13} = \frac{\partial u}{\partial z} + \frac{\partial w}{\partial x} = \frac{1}{\sqrt{G}} \left[\frac{\partial}{\partial \xi}(J_3 w) + \frac{\partial}{\partial \zeta}(u + J_1 w) \right],$$

$$D_{23} = \frac{\partial v}{\partial z} + \frac{\partial w}{\partial y} = \frac{1}{\sqrt{G}} \left[\frac{\partial}{\partial \eta}(J_3 w) + \frac{\partial}{\partial \zeta}(v + J_2 w) \right].$$

The turbulent mixing for potential temperature θ and water substances can be written in a general form for a scalar ϕ:

$$\begin{aligned} \sqrt{G}\, D_\phi &= \sqrt{G} \left(\frac{\partial H_1}{\partial x} + \frac{\partial H_2}{\partial y} + \frac{\partial H_3}{\partial z} \right) \\ &= \frac{\partial}{\partial \xi}(J_3 H_1) + \frac{\partial}{\partial \eta}(J_3 H_2) + \frac{\partial}{\partial \zeta}\left(H_3 + J_1 H_1 + J_2 H_2 \right) \end{aligned} \tag{6.3.5}$$

where H_1, H_2 and H_3 are horizontal and vertical turbulent fluxes of ϕ in the x, y and z directions respectively. These fluxes are defined by

$$\begin{aligned} H_1 &= \bar{\rho} K_{Hh} \frac{\partial \phi}{\partial x} = \bar{\rho} K_{Hh} \frac{1}{\sqrt{G}} \left[\frac{\partial}{\partial \xi}(J_3 \phi) + \frac{\partial}{\partial \zeta}(J_1 \phi) \right] \\ H_2 &= \bar{\rho} K_{Hh} \frac{\partial \phi}{\partial y} = \bar{\rho} K_{Hh} \frac{1}{\sqrt{G}} \left[\frac{\partial}{\partial \eta}(J_3 \phi) + \frac{\partial}{\partial \zeta}(J_2 \phi) \right] \\ H_3 &= \bar{\rho} K_{Hv} \frac{\partial \phi}{\partial z} = \bar{\rho} K_{Hv} \frac{1}{\sqrt{G}} \frac{\partial \phi}{\partial \zeta} \end{aligned} \tag{6.3.6}$$

where K_{Hh} and K_{Hv} are respectively horizontal and vertical mixing coefficients for ϕ. In general, the mixing coefficients are taken to be the same for heat, moisture, water or ice quantities. K_H equals K_m/Pr where Pr is the turbulent Prandtl number and is usually a constant having a value between 1/3 and 1.

The key to a turbulence closure scheme is the determination of the mixing coefficients. The Smagorinsky (1963) first-order closure scheme and the 1.5 order turbulent kinetic energy (TKE) based closure scheme are discussed in the following subsections. First, we discuss the spatial discretization of the formulations presented above.

As shown in Figure 6.1, variables τ_{11}, τ_{22}, τ_{33}, D_{11}, D_{22}, D_{33}, K_m and K_H are defined at the scalar point at the grid box center, H_1 at the u point, H_2

at the v point, and H_3 at the w point. τ_{13}, τ_{31} and D_{13} are defined at the same point as J_1. τ_{23}, τ_{32} and D_{23} are defined at the same point as J_2. τ_{12}, τ_{21} and D_{12} are defined half a grid interval to the right of v. Given this grid arrangement, the discretization of the turbulence terms are straightforward.

According to Eq. (6.3.4.),

$$
\begin{aligned}
D_{11} &= 2\frac{\partial u}{\partial x} = \frac{2}{\sqrt{G}}\left[\ \delta_\xi(\overline{J_3}^{\,\xi} u) + \ \delta_\zeta(\ \overline{J_1 \bar{u}^{\zeta}}^{\,\xi})\ \right] \\
D_{22} &= 2\frac{\partial v}{\partial y} = \frac{2}{\sqrt{G}}\left[\ \delta_\eta(\overline{J_3}^{\,\eta} v) + \ \delta_\zeta(\ \overline{J_2 \bar{v}^{\zeta}}^{\,\eta})\ \right] \\
D_{33} &= 2\frac{\partial w}{\partial z} = \frac{2}{\sqrt{G}}\ \delta_\zeta w \\
D_{12} &= \frac{1}{\overline{\overline{\sqrt{G}}^{\xi}}^{\eta}}\left[\ \delta_\eta(\overline{J_3}^{\,\xi} u) + \delta_\xi(\overline{J_3}^{\,\eta} v) + \ \delta_\zeta(\overline{J_2}^{\,\xi}\bar{u}^{\zeta\eta} + \overline{J_1}^{\,\eta}\bar{v}^{\zeta\xi}\ )\ \right] \\
D_{13} &= \frac{1}{\overline{\overline{\sqrt{G}}^{\xi}}^{\zeta}}\left[\ \ \delta_\xi(\overline{J_3}^{\,\zeta} w) + \ \delta_\zeta(u + \overline{J_1 \bar{w}^{\xi}}^{\,\zeta})\ \right] \\
D_{23} &= \frac{1}{\overline{\overline{\sqrt{G}}^{\eta}}^{\zeta}}\left[\ \ \delta_\eta(\overline{J_3}^{\,\zeta} w) + \ \delta_\zeta(v + \overline{J_2 \bar{w}^{\eta}}^{\,\zeta})\ \right].
\end{aligned}
\tag{6.3.7}
$$

The stresses τ_{ij} given in (6.3.2) are then obtained using D_{ij} with appropriate spatial averages of $\bar{\rho} K_m$,

$$
\begin{aligned}
\tau_{11} &= \bar{\rho} K_{mh}\ D_{11}\,, \\
\tau_{12} &= \overline{\bar{\rho} K_{mh}}^{\,\xi\eta}\ D_{12}\,, \\
\tau_{13} &= \overline{\bar{\rho} K_{mv}}^{\,\xi\zeta}\ D_{13}\,, \\
\tau_{21} &= \overline{\bar{\rho} K_{mh}}^{\,\eta\xi}\ D_{12}, \\
\tau_{22} &= \bar{\rho} K_{mh}\ D_{22}\,, \\
\tau_{23} &= \overline{\bar{\rho} K_{mv}}^{\,\eta\zeta}\ D_{23}\,, \\
\tau_{31} &= \overline{\bar{\rho} K_{mh}}^{\,\zeta\xi}\ D_{13}\,, \\
\tau_{32} &= \overline{\bar{\rho} K_{mh}}^{\,\zeta\eta} D_{23}\,, \\
\tau_{33} &= \bar{\rho} K_{mv}\ D_{33}\ .
\end{aligned}
\tag{6.3.8}
$$

where the velocity divergence, *Div* in τ_{11}, τ_{22} and τ_{33}, is calculated according to (6.3.2) at the scalar point

$$
Div = [\ \delta_\xi \{\overline{\sqrt{G}}^{\,\xi} u\ \} + \delta_\eta \{\overline{\sqrt{G}}^{\,\eta} v\ \} + \delta_\zeta \{\overline{\sqrt{G}}^{\,\zeta} W^c\}] \,/\, \sqrt{G}\ . \tag{6.3.9}
$$

The discretized form of the turbulent fluxes for scalars is

$$
\begin{aligned}
H_1 &= \overline{\left(\frac{\bar{\rho} K_{Hh}}{\sqrt{G}}\right)}^{\xi} \left[\delta_\xi (J_3\phi) + \delta_\zeta (J_1 \bar{\phi}^{\xi\zeta})\right], \\
H_2 &= \overline{\left(\frac{\bar{\rho} K_{Hh}}{\sqrt{G}}\right)}^{\eta} \left[\delta_\eta (J_3\phi) + \delta_\zeta (J_2 \bar{\phi}^{\eta\zeta})\right], \\
H_3 &= \overline{\left(\frac{\bar{\rho} K_{Hv}}{\sqrt{G}}\right)}^{\zeta} \delta_\zeta \bar{\phi}^{\zeta}\ .
\end{aligned}
\tag{6.3.10}
$$

Assuming that the mixing coefficient for momentum, K_m, can be determined and the mixing coefficient for temperature and water, K_H, is equal to K_m/Pr, then the turbulent mixing terms in (6.3.1) and (6.3.5) can be readily calculated from τ_{ij} and H_i from (6.3.8) and (6.3.10):

$$\sqrt{G}\, D_u = \delta_\xi\left(J_3\, \tau_{11}\right) + \delta_\eta\left(\overline{J_3}^{\xi\eta}\, \tau_{12}\right) + \delta_\zeta\left(\tau_{13} + J_1\, \overline{\tau_{11}}^{\xi\zeta} + \overline{\overline{J_2}^{\xi}\, \overline{\tau_{12}}^{\zeta}}^{\eta} \right)$$

$$\sqrt{G}\, D_v = \delta_\xi\left(\overline{J_3}^{\xi\eta}\ \tau_{21}\right) + \delta_\eta\left(J_3 \tau_{22}\right) + \delta_\zeta\left(\tau_{23} + \overline{\overline{J_1}^{\eta}\, \overline{\tau_{21}}^{\zeta}}^{\xi} + J_2\, \overline{\tau_{22}}^{\eta\zeta} \right)$$

$$\sqrt{G}\, D_w = \delta_\xi\left(\overline{J_3}^{\xi\zeta}\ \tau_{31}\right) + \delta_\eta\left(\overline{J_3}^{\eta\zeta} \tau_{32}\right) + \delta_\zeta\left(\tau_{33} + \overline{\overline{J_1}^{\zeta}\, \overline{\tau_{31}}^{\zeta}}^{\xi} + \overline{\overline{J_2}^{\zeta}\, \overline{\tau_{32}}^{\zeta}}^{\eta} \right) \quad (6.3.11)$$

and

$$\sqrt{G}\, D_\phi = \delta_\xi\left(\overline{J_3}^{\xi}\ H_1\right) + \delta_\eta\left(\overline{J_3}^{\eta} H_2\right) + \delta_\zeta\left(H_3 + \overline{\overline{H_1}^{\zeta}\, J_1}^{\xi} + \overline{\overline{H_2}^{\zeta}\, J_2}^{\eta} \right) . \quad (6.3.12)$$

6.3.3. Smagorinsky first-order closure

The key to a turbulence closure scheme is the determination of the mixing coefficients. The modified Smagorinsky scheme (Smagorinsky, 1963; Lilly, 1962) defines $K_{mh} = K_{mv} = K_m$ as

$$K_m = (k\,\Delta)^2\, [\, \max(\, |Def\,|^2 - N^2/\mathrm{Pr}\, ,\, 0\,)\,]^{1/2} \quad (6.3.13)$$

where k is an empirical constant and takes a value of 0.21 after Deardorff (1972a). Δ is the a measure of the grid scale. On a model grid with similar grid spacing in all three directions, the turbulence is nearly isotropic,

$$\Delta = (\Delta x\, \Delta y\, \Delta z)^{1/3}. \quad (6.3.14)$$

When the grid aspect ratio ($\Delta x / \Delta z$) is on the order of 10 or larger, as is often the case when high vertical resolution is required in the boundary layer, K_{mv} as determined according to (6.3.13) and (6.3.14) can become too large, resulting in excessive vertical mixing. This artificially strong vertical mixing is found to destroy the base state environment when the environment is not stable enough to suppress the turbulence. The larger vertical coefficient also imposes a severe computational stability constraint on the large time step size. This issue is addressed by using different length scales for the horizontal and vertical directions, so that

$$K_{mh} = (k\,\Delta_h)^2\, [\, \max(\, |Def\,|^2 - N^2/\mathrm{Pr}\, ,\, 0\,)\,]^{1/2}, \quad (6.3.15)$$

$$K_{mv} = (k\,\Delta_v)^2\, [\, \max(\, |Def\,|^2 - N^2/\mathrm{Pr}\, ,\, 0\,)\,]^{1/2},$$

where

$$\Delta_h = (\Delta x \, \Delta y)^{1/2} \quad and \quad \Delta_v = \Delta z \tag{6.3.16}$$

We refer to this case as an anisotropic turbulence case. A similar approach is taken by Tripoli and Cotton (1982).

The magnitude of deformation |*Def*| in (6.3.13) is given by

$$|Def|^2 = \frac{1}{2}\left(D_{11}^2 + D_{22}^2 + D_{33}^2 \right) + D_{12}^2 + D_{13}^2 + D_{23}^2 - \frac{2}{3} Div^2 . \tag{6.3.17}$$

In (6.3.13) and (6.3.15), N^2 is the Brunt-Väisälä frequency

$$N^2 = \begin{cases} \dfrac{g}{\sqrt{G}} \dfrac{\partial \ln\theta}{\partial \zeta} & for\ q_v < q_{vs} \\ \dfrac{g}{\sqrt{G}} \left[\dfrac{1 + Lq_{vs}/(RT)}{1 + L^2 q_{vs}/(C_p R_v T^2)} \left(\dfrac{\partial \ln\theta}{\partial \zeta} + \dfrac{L}{C_p T} \dfrac{\partial q_{vs}}{\partial \zeta} \right) - \dfrac{\partial q_w}{\partial \zeta} \right] & for\ q_v \geq q_{vs} \end{cases} \tag{6.3.18}$$

where q_{vs} is the saturation mixing ratio and q_w the total water mixing ratio. L the latent heat of vaporization, R the gas constant for dry air, R_v the gas constant for water vapor and C_p the specific heat for dry air at constant pressure. When the air becomes saturated, the moist static stability replaces the dry stability, and the formula for the moist static stability in (6.3.15) follows Durran and Klemp (1982). The contribution of ice processes to (6.3.18) are neglected.

The saturation mixing ratio q_{vs} is calculated using Teten's formula

$$q_{vs} = \frac{380}{p} \exp\left(a_w \frac{T\text{-}273.16}{T - b_w} \right) \tag{6.3.19}$$

where

$$\begin{aligned} &a_w = 17.27 \text{ and } b_w = 35.5 \text{ for } T \geq 273.16\ K \\ &a_w = 21.875 \text{ and } b_w = 7.5 \text{ for } T < 273.16\ K. \end{aligned} \tag{6.3.20}$$

The cell-centered deformation in (6.3.17) is calculated according to

$$|Def|^2 = \frac{1}{2}\left(D_{11}^2 + D_{22}^2 + D_{33}^2 \right) + \left(\overline{D_{12}}^{\xi\eta} \right)^2 + \left(\overline{D_{13}}^{\xi\zeta} \right)^2 + \left(\overline{D_{23}}^{\eta\zeta} \right)^2 \tag{6.3.21}$$

and the cell-centered Brunt-Väisälä frequency N is calculated according to

$$N^2 = \begin{cases} \dfrac{g}{\sqrt{G}} \dfrac{1}{\theta} \delta_\zeta \bar{\theta}^\zeta & for\ q_v < q_{vs} \\ \dfrac{g}{\sqrt{G}} \left[\dfrac{1 + Lq_{vs}/(RT)}{1 + L^2 q_{vs}/(C_p R_v T^2)} \left(\dfrac{1}{\theta} \delta_\zeta \bar{\theta}^\zeta + \dfrac{L}{C_p T} \delta_\zeta \overline{q_{vs}}^\zeta \right) - \delta_\zeta \overline{q_w} \right] & for\ q_v \geq q_{vs} \end{cases} \tag{6.3.22}$$

K_m can then be readily calculated from (6.3.15), and it is done at the scalar point. The mixing coefficient for temperature and water is $K_H = K_m/Pr$, where Pr is the Prandtl number.

6.3.4. 1.5-order turbulent kinetic energy-based closure scheme

With this scheme, the turbulent mixing coefficient is related to the turbulent kinetic energy E ($\equiv \overline{u'^2 + v'^2 + w'^2}/2$) instead of the deformation and static stability as in the Smagorinsky closure scheme. In this case, an additional prognostic equation for the turbulent kinetic energy, E, is solved, which is

$$\begin{aligned} \frac{\partial \rho^* E}{\partial t} &= -\left(u^* \frac{\partial E}{\partial \xi} + v^* \frac{\partial E}{\partial \eta} + W^{c*} \frac{\partial E}{\partial \zeta} \right) + C \\ &+ \rho^* \left(K_m |Def|^2 - \frac{2}{3} E\, Div \right) - \rho^* \frac{C_\varepsilon}{l} E^{2/3} \\ &+ 2 \left[\frac{\partial}{\partial \xi}(J_3 H_1) + \frac{\partial}{\partial \eta}(J_3 H_2) + \frac{\partial}{\partial \zeta}\left(H_3 + J_1 H_1 + J_2 H_2 \right) \right] \end{aligned} \tag{6.3.23}$$

The terms on the right hand side are, respectively, the advection, potential-kinetic energy conversion, shear production, dissipation and diffusion of turbulent kinetic energy. The formulation of the diffusion term, is similar to those for heat and moisture. In (6.3.23), the turbulent flux components are:

$$H_1 = \bar{\rho} K_{mh} \frac{\partial E}{\partial x} = \frac{\bar{\rho} K_{mh}}{\sqrt{G}} \left[\frac{\partial}{\partial \xi} (J_3 E) + \frac{\partial}{\partial \zeta} (J_1 E) \right]$$

$$H_2 = \bar{\rho} K_{mh} \frac{\partial E}{\partial y} = \frac{\bar{\rho} K_{mh}}{\sqrt{G}} \left[\frac{\partial}{\partial \eta} (J_3 E) + \frac{\partial}{\partial \zeta} (J_2 E) \right] \qquad (6.3.24)$$

$$H_3 = \bar{\rho} K_{mv} \frac{\partial E}{\partial z} = \frac{\bar{\rho} K_{mv}}{\sqrt{G}} \frac{\partial E}{\partial \zeta}$$

The potential-kinetic energy conversion term C is given by

$$C = \begin{cases} -g \left[A \rho^* K_{Hv} \dfrac{\partial \theta_e}{\partial \zeta} - \rho^* K_{Hv} \dfrac{\partial q_{ls}}{\partial \zeta} \right] & for\ q_v \geq q_s\ or\ q_c > 0 \\ -g \rho^* K_{Hv} \left[\dfrac{1}{\theta} \dfrac{\partial \theta}{\partial \zeta} + 0.61 \dfrac{\partial q_v}{\partial \zeta} \right] & for\ q_v < q_s\ or\ q_c = 0 \end{cases} \qquad (6.3.25)$$

in which A is defined as

$$A = \frac{1}{\bar{q}} \frac{1 + \dfrac{1.61\, \varepsilon L q_v}{R\bar{T}}}{1 + \dfrac{\varepsilon L^2 q_v}{C_p R \bar{T}^2}} \qquad (6.3.26)$$

with ε=0.622; q_{ls} is the sum of all vapor, liquid and solid water substances, and θ_e is the equivalent potential temperature.

In the dissipation term, coefficient C_ε has the value

$$C_\varepsilon = \begin{cases} 3.9 & \text{at lowest level,} \\ 0.93 & \text{otherwise.} \end{cases} \qquad (6.3.27)$$

The mixing coefficients K_{mh} and K_{mh} are functions of E and the length scales:

$$K_{mh} = 0.1\, E^{1/2}\, l_h \text{ and } K_{mv} = 0.1\, E^{1/2}\, l_v \qquad (6.3.28)$$

For a grid distribution with an aspect ratio on the order of unity, the horizontal length scale l_h and the vertical length scale l_v are the same, and are given by (Deardorff, 1980)

$$l = l_h = l_v = \begin{cases} \Delta s \quad \textit{for unstable or neutral case,} \\ \min(\Delta s, l_s) \quad \textit{for stable case.} \end{cases} \tag{6.3.29}$$

where $\Delta s = (\Delta x\, \Delta y \Delta z)^{1/3}$ and l_s is defined as

$$l_s = 0.76 E^{1/2} \left| \frac{g}{\bar{\theta}} \frac{\partial \bar{\theta}}{\partial z} \right|^{-1/2}.$$

For a grid distribution with very large aspect ratio,

$$l_h = \Delta s_h$$

and

$$l_v = \begin{cases} \Delta s_v \quad \textit{for an unstable or neutral case,} \\ \min(\Delta s_v, l_s) \quad \textit{for a stable case.} \end{cases} \tag{6.3.30}$$

where $\Delta s_h = (\Delta x\, \Delta y)^{1/2}$ and $\Delta s_v = \Delta z$.

The turbulent Prandtl number ($Pr = K_m/K_H$) is given by

$$\Pr = \frac{K_m}{K_H} = \frac{1}{1 + \dfrac{2l_v}{\Delta s_v}} \tag{6.3.31}$$

therefore K_H becomes available once K_m is known. Note that we plan to add another option of computing K_m and K_H according to Schumann (1991) in the near future.

In (6.3.23), the advection and diffusion terms are similar to those in the other scalar equations (*e.g.*, Eq.(6.3.26)), they can be calculated in a similar way. It is worth noting that if E is zero everywhere at a given time, E will remain zero ever after according to (6.3.23). To remedy this, we check the local Richardson number $Ri = N^2 / |Def|^2$. If it falls below a critical Richardson number, turbulence activity is expected and we impose a lower limit on E, i.e.,

$$\begin{aligned} K_{mh} &= \max\left(0.1 E^{1/2} l_h, \alpha \Delta s_h^2\right), \\ K_{mv} &= \max\left(0.1 E^{1/2} l_v, \alpha \Delta s_v^2\right). \end{aligned} \tag{6.3.32}$$

where α is a small number (*e.g.*, α=10^{-6}).

6.3.5. Dynamic eddy viscosity model - Germano scheme

In the widely used Smagorinsky closure method discussed in Section 6.3.3, an empirical constant, C_S is employed. However, the considerable variation of C_S evident in real flows, limits the utility of this closure method. In addition, the computed eddy viscosity does not vanish in laminar flow or at solid boundaries, as is observed.

In ARPS, we can use an optional dynamic model to convert previously prescribed SGS model coefficients to self-determined parameters that vary with time and space (Germano *et al.*, 1991; Wong, 1992; Wong and Lilly, 1994; Wong, 1994). Within a simulation, the SGS representation is locally and dynamically adjusted to match the statistical structure of the smallest resolvable eddies.

The dynamic SGS model (Wong and Lilly, 1994) expresses the total SGS stress tensor, $\tau_{ij}\ (\equiv \overline{u_i u_j} - \bar{u}_i \bar{u}_j)$, and temperature flux, $\tau_{\theta i}\ (\equiv \overline{\theta u_i} - \bar{\theta}\,\bar{u}_i)$ as:

$$\tau_{ij} - \frac{\delta_{ij}}{3}\tau_{kk} = -2\nu_t \left(\overline{S_{ij}} - \frac{\delta_{ij}}{3}\overline{S_{kk}}\right) \tag{6.3.33}$$

$$\tau_{\theta i} = -\nu_\theta \frac{\partial \bar{\theta}}{\partial x_i}, \tag{6.3.34}$$

where $\overline{S_{ij}} \equiv \left(\partial \overline{u_i}/\partial x_j + \partial \overline{u_j}/\partial x_i\right)/2$ is the resolved strain rate tensor. Here the overbar represents an averaging on the grid scale, *i.e.*, the smallest resolved scale. According to Kolmogorov scaling, the eddy viscosity ν_t and eddy diffusivity ν_θ can be defined as

$$\nu_t = C\overline{\Delta}^{4/3}, \tag{6.3.35}$$

$$\nu_\theta = \frac{C}{Pr}\overline{\Delta}^{4/3}, \tag{6.3.36}$$

where the model coefficient, C, and the eddy Prandtl number, Pr, are assumed to be independent of the grid-filter width, $\overline{\Delta}\ (\equiv (\Delta x_1 \Delta x_2 \Delta x_3)^{1/3})$, with $x_i\ (i = 1,2,3)$ being the grid spacing in the *i*th direction. The model

coefficients, C and Pr, are determined by using the dynamic SGS closure developed by Germano *et al.* (1991) and modified by Lilly (1992).

The main premise behind dynamic SGS modeling is the use of information at two different resolved scales to evaluate the model coefficients. We therefore introduce a second spatial filter, with a larger filter width than the grid filter, called the "test filter". This filter generates a second set of resolvable-scale fields (denoted by ^). The test-filtered flow quantities are obtained by volume-averaging the grid-scale variables over 27 grid cells, within a test-filtering volume, using a stencil of 3 grid points in each direction. We also choose the test-filter scale $\hat{\Delta} = 2\overline{\Delta}$ which is consistent with other 3-D filtering models.

By direct analogy to (6.3.36), the subtest-scale (STS) stress tensor T_{ij} is T_{ij} $\left(\equiv \widehat{\overline{u_i}\overline{u_j}} - \hat{\bar{u}}_i\hat{\bar{u}}_j\right)$ approximated by

$$T_{ij} - \delta_{ij} T_{kk}/3 = -2\nu_T \left(\hat{\bar{S}}_{ij} - \delta_{ij} \hat{\bar{S}}_{kk}/3\right) \tag{6.3.37}$$

where $\hat{\bar{S}}_{ij} \equiv \left(\partial\hat{\bar{u}}_i/\partial x_j + \partial\hat{\bar{u}}_j/\partial x_i\right)/2$ and $\nu_T \left(\approx C\hat{\Delta}^{4/3}\right)$ is the STS eddy viscosity. Similarly, the STS temperature flux $T_{\theta i}$ $\left(\equiv \widehat{\overline{\theta}\overline{u}_i} - \hat{\bar{\theta}}\hat{\bar{u}}_i\right)$ is given by

$$T_{\theta i} = -\nu_\theta \frac{\partial\hat{\bar{\theta}}}{\partial x_i}, \tag{6.3.38}$$

where $\nu_\theta \left(\approx C\hat{\Delta}^{4/3}/Pr\right)$ is the STS eddy diffusivity. The fluxes, τ_{ij}, $\tau_{\theta i}T_{ij}$ and $T_{\theta i}$, are unknown quantities because $\overline{u_i u_j}$, $\overline{\theta u_i}$, $\widehat{\overline{u_i}\overline{u_j}}$ and $\widehat{\overline{\theta}\overline{u_i}}$ contain information within the unresolved scale. However, subtracting the test-scale average of τ_{ij} and $\tau_{\theta i}$ from T_{ij} and $T_{\theta i}$, respectively, leads to

$$L_{ij} \equiv T_{ij} - \hat{\tau}_{ij} = \widehat{\overline{u_i}\overline{u_j}} - \hat{\bar{u}}_i\hat{\bar{u}}_j, \tag{6.3.39}$$

and

$$R_{\theta i} \equiv T_{\theta i} - \hat{\tau}_{\theta i} = \widehat{\overline{\theta}\overline{u_i}} - \hat{\bar{\theta}}\hat{\bar{u}}_j. \tag{6.3.40}$$

The test window elements L_{ij} and $R_{\theta i}$ are known quantities because the right hand side of (6.3.39) and (6.3.40) can be directly evaluated from the resolved velocity and temperature fields. According to (6.3.36), (6.3.35), (6.3.37), and (6.3.39),

$$L_{ij} - \delta_{ij} L_{kk} / 3 \approx 2 C M_{ij}, \tag{6.3.41}$$

with $M_{ij} \equiv (\Delta^{-4/3} - \hat{\Delta}^{4/3})(\hat{\bar{S}}_{ij} - \delta_{ij} \hat{\bar{S}}_{kk} / 3)$. Since $L_{ij} = L_{ji}$, (6.3.41) represents six independent equations with one unknown, C. As (6.3.41) is an overdetermined system, it is appropriate to use a least squares method to determine C:

$$2\Delta^{-4/3} C \approx \frac{\left\langle (L_{ij} - \delta_{ij} L_{kk} / 3)(\hat{\bar{S}}_{ij} - \delta_{ij} \hat{\bar{S}}_{kk} / 3) \right\rangle}{(1 - \left[\hat{\Delta} / \bar{\Delta}\right]^{4/3}) \left\langle (\hat{\bar{S}}_{lm} - \delta_{lm} \hat{\bar{S}}_{nn} / 3)^2 \right\rangle} \tag{6.3.42}$$

where $\langle\ \rangle$ indicates local volume averaging, and the summation convention is in effect.

Similarly,

$$\Delta^{-4/3} \frac{C}{\mathrm{Pr}} \approx \frac{\left\langle R_{\theta i} \frac{\partial \hat{\bar{\theta}}}{\partial x_j} \right\rangle}{\left(1 - \left[\hat{\Delta} / \bar{\Delta}\right]^{4/3}\right) \left\langle \left(\frac{\partial \hat{\bar{\theta}}}{\partial x_j}\right)^2 \right\rangle}. \tag{6.3.43}$$

One can divide (6.3.42) by (6.3.43) to obtain the eddy Prandtl number Pr.

To close the system for compressible fluids, we need to compute τ_{kk} in (6.3.36). By analogy to the expression introduced by Yoshizawa (1984) , we need to compute τ_{kk}:

$$\tau_{kk} = 2 C_I \bar{\Delta}^{4/3} \bar{S}. \tag{6.3.44}$$

where $\bar{S} \equiv (2 \bar{S}_{ij} \bar{S}_{ij}^{1/2})$ is a measurement of the resolved strain rate tensor $\bar{S}_{ij}$. Making use of the trace of (6.3.39) with the model of (6.3.44) for T_{kk} and τ_{kk}, we obtain

$$2\bar{\Delta}^{4/3} C_I \approx \frac{L_{kk}}{\left(\left[\hat{\Delta} / \bar{\Delta}\right]^{4/3} - 1\right) \langle \hat{\bar{S}} \rangle}. \tag{6.3.45}$$

According to (6.3.39), L_{kk} in (6.3.45) is non-negative since the average of the square of a quantity is never less than the square of its average. It follows that $C_I \geq 0$ and thus a realizability condition, $\tau_{kk} \geq 0$, is satisfied.

Eqs. (6.3.36)-(6.3.36), and (6.3.42)-(6.3.45) form a closed SGS system with the filter width ratio $\hat{\Delta}/\overline{\Delta}$ being the only input parameter. The denominator of (6.3.42) can vanish only if each component of $\hat{\bar{S}}_{ij}$ vanishes separately. In that case, the numerator also vanishes. A similar conclusion applies to (6.3.43). Moreover, at a solid boundary or for laminar flow, L_{ij} vanishes and according to (6.3.42)-(6.3.45), all the SGS model coefficients also vanish.

6.4. Computational Mixing / Numerical Smoothing

The subgrid scale mixing provides smoothing related to turbulent processes only in the region where $K_m > 0$. In stable regions where K_m is zero, there is no turbulent mixing. A small amount of background (computational) mixing is desirable to discourage the growth of nonlinear instabilities and to suppress small scale computational noise. This can be achieved by either adding a constant to the coefficient of the physical (subgrid scale turbulence) mixing, or by introducing an additional mixing / smoothing term on the right hand side of the conservation equations (except for pressure). We refer to the latter as computational mixing.

To ensure computational stability, all mixing / damping / diffusion terms are evaluated at the previous time level of the time integration. This makes the scheme forward in time with respect to the mixing terms. It is important to note that the time integration of the terms is conditionally stable. Under certain circumstances, the constraint on the time step size imposed by these terms can be more severe that by other processes, such as gravity wave propagation and advection.

In the following subsections, several optional computational mixing formulations as well as upper level Rayleigh damping formulations are discussed.

6.4.1. Constant background mixing in physical space

This type of mixing is included by adding a user-specified constant, K_{mB}, to the mixing coefficient, K_m, that is calculated in the previous section. The total mixing on scalars will be $K_H + K_{HB} = (K_m + K_{mB})/Pr$. Because this mixing operates on the total fields, it tends to diffuse the environmental and perturbation fields' shear and stratification. This property may not be desirable

in many cases. The choice of the background mixing coefficient follows a guideline similar to that for the second-order computational mixing.

6.4.2. Numerical smoothing in the computational space

This type of computational smoothing is designed to remove the small scale (mainly grid scale) noise of computational origin (*e.g.*, advection-induced overshoots and undershoots, energy cascade towards small scales due to nonlinear instability). It is therefore designed to operate along computational grid lines (ξ, η and ζ) instead of the physical coordinate lines (x, y and z). To avoid the unwanted effect of smoothing the base-state fields (thus destroying the environmental stratification), the smoothing is formulated to operate on the perturbations (u', v', w, θ' and q'_ψ) only. Therefore, this smoothing tends to relax the total fields towards the base-state values. Because of its non-physical origin, the computational smoothing should be as small as possible in order to avoid affecting the physical solution.

ARPS offers second- and fourth-order computational mixing. Fourth order mixing is preferred because it damps out short wavelength noise more selectively than the second order mixing. Theoretically, the higher the order of smoothing, the more strongly the short wavelengths are damped. In practice, however, high order smoothing is more difficult to implement, especially near the boundaries.

With the total mixing divided into separate parts, the conservation equations may be written like this:

$$\frac{\partial(\rho^* \phi)}{\partial t} = \sqrt{G}\ (D_{\phi 1} + D_{\phi 2} + D_{\phi 3}) + ... \qquad (6.4.1)$$

where $D_{\phi 1}$ represents the subgrid scale turbulent mixing, $D_{\phi 2}$ the second and/or fourth order computational mixing and $D_{\phi 3}$ the upper-level Rayleigh type damping. Here ϕ is one of u, v, w, θ, or one of the water or ice variables.

a) Second order computational mixing

In ARPS, the second order mixing has the following form:

$$\sqrt{G}\, D_{\phi 2} = K_{H2}\left[\frac{\partial^2(\bar{\rho}\phi')}{\partial\xi^2} + \frac{\partial^2(\bar{\rho}\phi')}{\partial\eta^2}\right] + K_{V2}\frac{\partial^2(\bar{\rho}\phi')}{\partial\zeta^2} \tag{6.4.2}$$

where $\phi' = \phi - \bar{\phi}$ is the perturbation of ϕ from its base-state value. K_{H2} and K_{V2} are the horizontal and vertical mixing coefficients, respectively. Equation (6.4.2) contains conservative terms which operate along the computational rather than the physical (Cartesian) grid lines.

To discretize (6.4.2) in the finite difference form, it is convenient to define a finite difference operator

$$\delta_s^2\phi = \frac{\phi_{i+1} - 2\phi_i + \phi_{i-1}}{\Delta s^2} \tag{6.4.3}$$

where s denotes one of the independent variables ξ, η or ζ. The finite-differenced formulations of Eq. (6.4.2) for *u, v, w* and scalar *S* become

$$\begin{aligned}
\sqrt{G}\, D_{u2} &= K_{H2}\left[\delta_\xi^2(\bar{\bar{\rho}}^{\xi}u') + \delta_\eta^2(\bar{\bar{\rho}}^{\xi}u')\right] + K_{V2}\left[\delta_\zeta^2(\bar{\bar{\rho}}^{\xi}u')\right] \\
\sqrt{G}\, D_{v2} &= K_{H2}\left[\delta_\xi^2(\bar{\bar{\rho}}^{\eta}v') + \delta_\eta^2(\bar{\bar{\rho}}^{\eta}v')\right] + K_{V2}\left[\delta_\zeta^2(\bar{\bar{\rho}}^{\eta}v')\right] \\
\sqrt{G}\, D_{w2} &= K_{H2}\left[\delta_\xi^2(\bar{\bar{\rho}}^{\zeta}w) + \delta_\eta^2(\bar{\bar{\rho}}^{\zeta}w)\right] + K_{V2}\left[\delta_\zeta^2(\bar{\bar{\rho}}^{\zeta}w)\right] \\
\sqrt{G}\, D_{S2} &= K_{H2}\left[\delta_\xi^2(\bar{\rho}S') + \delta_\eta^2(\bar{\rho}S')\right] + K_{V2}\left[\delta_\zeta^2(\bar{\rho}S')\right].
\end{aligned} \tag{6.4.4}$$

These terms are evaluated at the interior points of the model domain without application of boundary conditions. The horizontal mixing coefficien,t K_{H2} , equals $\alpha_{H2}\,\Delta_H^2/\Delta t$, where α_{H2} is a non-dimensional coefficient; Δ_H is the horizontal grid scale taken as $(\Delta x \Delta y)^{1/2}$. Similarly, $K_{v2} = \alpha_{v2}\,\Delta_v^2/\Delta t$, where α_{v2} is a non-dimensional coefficient and $\Delta_v = \Delta\zeta$. For computational stability, α_{H2} and α_{v2} must be less than or equal to 1/8. The dimensional (1/s) ratios $K_{H2}/\Delta_{\mathrm{H}}^2$ and $K_{v2}/\Delta_{\mathrm{v}}^2$ are specified by the user in theinput file.

b) Fourth order computational mixing

The fourth order computational mixing terms have the form

$$\sqrt{G}\, D_{\phi 2} = - K_{H4} \left[\frac{\partial^4(\bar{\rho}\phi')}{\partial \xi^4} + \frac{\partial^4(\bar{\rho}\phi')}{\partial \eta^4} \right] - K_{V4} \left[\frac{\partial^4(\bar{\rho}\phi')}{\partial \zeta^4} \right] . \qquad (6.4.5)$$

The finite differenced formulations for u, v, w and any scalar, S, (representing θ and the water and ice categories) are

$$\sqrt{G}\, D_{u2} = - K_{H4} \left\{ \delta_\xi^2 \left[\delta_\xi^2 (\bar{\bar{\rho}}^{\xi} u') \right] + \delta_\eta^2 \left[\delta_\eta^2 (\bar{\bar{\rho}}^{\xi} u') \right] \right\} - K_{V4}\, \delta_\zeta^2 \left[\delta_\zeta^2 (\bar{\bar{\rho}}^{\xi} u') \right] ,$$

$$\sqrt{G}\, D_{v2} = - K_{H4} \left\{ \delta_\xi^2 \left[\delta_\xi^2 (\bar{\bar{\rho}}^{\eta} v') \right] + \delta_\eta^2 \left[\delta_\eta^2 (\bar{\bar{\rho}}^{\eta} v') \right] \right\} - K_{V4}\, \delta_\zeta^2 \left[\delta_\zeta^2 (\bar{\bar{\rho}}^{\eta} v') \right] ,$$

$$\sqrt{G}\, D_{w2} = - K_{H4} \left\{ \delta_\xi^2 \left[\delta_\xi^2 (\bar{\bar{\rho}}^{\zeta} w) \right] + \delta_\eta^2 \left[\delta_\eta^2 (\bar{\bar{\rho}}^{\zeta} w) \right] \right\} - K_{V4}\, \delta_\zeta^2 \left[\delta_\zeta^2 (\bar{\bar{\rho}}^{\zeta} w) \right] ,$$

$$\sqrt{G}\, D_{S2} = - K_{H4} \left\{ \delta_\xi^2 \left[\delta_\xi^2 (\bar{\rho} S') \right] + \delta_\eta^2 \left[\delta_\eta^2 (\bar{\rho} S') \right] \right\} - K_{V4}\, \delta_\zeta^2 \left[\delta_\zeta^2 (\bar{\rho} S') \right] . \qquad (6.4.6)$$

The fourth-order terms given above cannot be directly evaluated at the first grid point inside the boundary. Therefore, either a second order substitute or prespecified boundary condition must be applied. The former may introduce erroneous sources or sinks at the transition between the two schemes. In ARPS, we overcome this difficulty by making additional assumptions for the intermediate terms such as $\delta_\xi^2(\bar{\bar{\rho}}^{\xi} u')$. In this way, the mixing terms can be evaluated up to the first grid point inside the boundary, and the formulation retains its conservative property. In the case of symmetric or periodic boundary conditions, however, no artificial assumptions are needed.

The fourth-order mixing terms given in (6.4.6) are computed in two steps. First, the terms in the squared brackets are evaluated at the interior grid points of the model domain, and their values at the boundaries are set based on additional assumptions. The mixing terms are then calculated from these intermediate terms, up to the first grid point inside the boundaries. Splitting the calculations into two steps also results in modular calculations, where each

path through the operator involves only three grid points in each direction. This approach follows the massively parallel implementation of the code.

Denoting

$$
\begin{aligned}
D2XIU &= \delta_\xi^2(\bar{\rho}^\xi u'), & D2ETAU &= \delta_\eta^2(\bar{\rho}^\xi u'),\\
D2XIV &= \delta_\xi^2(\bar{\rho}^\eta v'), & D2ETAV &= \delta_\eta^2(\bar{\rho}^\eta v'),\\
D2XIW &= \delta_\xi^2(\bar{\rho}^\zeta w'), & D2ETAW &= \delta_\eta^2(\bar{\rho}^\zeta w'),\\
D2XIS &= \delta_\xi^2(\bar{\rho} S'), & D2ETAS &= \delta_\eta^2(\bar{\rho} S'),
\end{aligned}
\qquad (6.4.7)
$$

we set the boundary conditions for the second derivatives for the symmetric (wall) boundaries as

$$
\begin{aligned}
&D2XIU(1,j,k) = -\,D2XIU(3,j,k) && \text{for all } j \text{ and } k;\\
&D2XIU(nx,j,k) = -\,D2XIU(nx-2,j,k) && \text{for all } j \text{ and } k;\\
&D2ETAU(i,1,k) = D2ETAU(i,2,k) && \text{for all } i \text{ and } k;\\
&D2ETAU(i,ny-1,k) = D2ETAU(i,ny-2,k) && \text{for all } i \text{ and } k.\\
&\\
&D2XIV(1,j,k) = D2XIV(2,j,k) && \text{for all } j \text{ and } k;\\
&D2XIV(nx-1,j,k) = D2XIV(nx-2,j,k) && \text{for all } j \text{ and } k;\\
&D2ETAV(i,1,k) = -\,D2ETAV(i,3,k) && \text{for all } i \text{ and } k;\\
&D2ETAV(i,ny,k) = -\,D2ETAV(i,ny-2,k) && \text{for all } i \text{ and } k.\\
&\\
&D2XIW(1,j,k) = D2XIW(2,j,k) && \text{for all } j \text{ and } k;\\
&D2XIW(nx-1,j,k) = D2XIW(nx-2,j,k) && \text{for all } j \text{ and } k;\\
&D2ETAW(i,1,k) = D2ETAW(i,2,k) && \text{for all } i \text{ and } k;\\
&D2ETAW(i,ny-1,k) = D2ETAW(i,ny-2,k) && \text{for all } i \text{ and } k,
\end{aligned}
\qquad (6.4.8)
$$

and for the periodic boundaries:

$$
\begin{aligned}
&D2XIU(1,j,k) = D2XIU(nx-2,j,k) && \text{for all } j \text{ and } k;\\
&D2XIU(nx,j,k) = D2XIU(3,j,k) && \text{for all } j \text{ and } k;\\
&D2ETAU(i,1,k) = D2ETAU(i,ny-2,k) && \text{for all } i \text{ and } k;\\
&D2ETAU(i,ny-1,k) = D2ETAU(i,2,k) && \text{for all } i \text{ and } k;\\
&\\
&D2XIV(1,j,k) = D2XIV(nx-2,j,k) && \text{for all } j \text{ and } k;\\
&D2XIV(nx-1,j,k) = D2XIV(2,j,k) && \text{for all } j \text{ and } k;\\
&D2ETAV(i,1,k) = D2ETAV(i,ny-2,k) && \text{for all } i \text{ and } k;\\
&D2ETAV(i,ny,k) = D2ETAV(i,3,k) && \text{for all } i \text{ and } k;\\
&\\
&D2XIW(1,j,k) = D2XIW(nx-2,j,k) && \text{for all } j \text{ and } k;\\
&D2XIW(nx-1,j,k) = D2XIW(2,j,k) && \text{for all } j \text{ and } k;
\end{aligned}
\qquad (6.4.9)
$$

D2ETAW(i,1,k) = *D2ETAW(i,ny-2,k)* for all *i* and *k;*
D2ETAW(i,ny-1,k) = *D2ETAW(i,2,k)* for all *i* and *k.*

The conditions on the lateral boundaries for a scalar *S* are exactly the same as those for *w*.

For zero gradient and open boundary conditions, we simply set the normal gradient of the second order terms to zero at the boundaries, *i.e.*

D2XIU(1,j,k) = *D2XIU(2,j,k)* for all *j* and *k;*
D2XIU(nx,j,k) = *D2XIU(nx-1,j,k)* for all *j* and *k;*
D2ETAU(i,1,k) = *D2ETAU(i,2,k)* for all *i* and *k;*
D2ETAU(i,ny-1,k) = *D2ETAU(i,ny-2,k)* for all *i* and *k;*

D2XIV(1,j,k) = *D2XIV(2,j,k)* for all *j* and *k;*
D2XIV(nx-1,j,k) = *D2XIV(nx-2,j,k)* for all *j* and *k;*
D2ETAV(i,1,k) = *D2ETAV(i,2,k)* for all *i* and *k;*
D2ETAV(i,ny,k) = *D2ETAV(i,ny-1,k)* for all *i* and *k;* (6.4.10)

D2XIW(1,j,k) = *D2XIW(2,j,k)* for all *j* and *k;*
D2XIW(nx-1,j,k) = *D2XIW(nx-2,j,k)* for all *j* and *k;*
D2ETAW(i,1,k) = *D2ETAW(i,2,k)* for all *i* and *k;*
D2ETAW(i,ny-1,k) = *D2ETAW(i,ny-2,k)* for all *i* and *k;*

D2XIS(1,j,k) = *D2XIS(2,j,k)* for all *j* and *k;*
D2XIS(nx-1,j,k) = *D2XIS(nx-2,j,k)* for all *j* and *k;*
D2ETAS(i,1,k) = *D2ETAS(i,2,k)* for all *i* and *k;*
D2ETAS(i,ny-1,k) = *D2ETAS(i,ny-2,k) f* for all *i* and *k.*

The vertical mixing terms are treated in a similar manner.

c) Assigning the mixing coefficients

The fourth order horizontal smoothing coefficient K_{H4} can be expressed as $\alpha_{H4}\Delta_H^4/\Delta t$. Here α_{H4} is the non-dimensional coefficient and Δ_H the horizontal grid scale taken as $(\Delta x\, \Delta y)^{1/2}$. Δt is the large time step size. The vertical coefficient K_{V4} equals $\alpha_{V4}\Delta_V^4/\Delta t$. A value of 0.001 is typically used for α. The same value of α for the second order mixing produces a similar amount of damping on the grid scale noises. Again, it is important to note, that *the mixing terms using forward-in-time integration schemes are only conditionally stable. Excessively large mixing coefficients will lead to computational instability*. A discussion on the computational stability of diffusive formulations is presented by Pielke (1984).

6.4.3. Upper boundary damping layer

Enhanced damping is can be optionally included in a layer near the top boundary in order to absorb upward propagating wave disturbances and to eliminate wave reflection at the top boundary. Preventing wave reflection at the top boundary is especially important in the studies of terrain-induced flows.

Rayleigh damping adds an additional term to the RHS of the conservation equations of momentum, potential temperature and water and ice quantities. It damps the perturbations from the base state. These terms are represented by $D_{\phi 3}$ in Eq. (6.4.1), and have the form

$$\sqrt{G}\, D_{\phi 3} = - R_D(z)\, \rho^* (\phi - \bar{\phi}) \tag{6.4.11}$$

where R_D is the vertical profile of the inverse damping time scale, and ϕ is u, v, w, θ or a water substance.

ARPS applies the profile of R_D suggested by Klemp and Lilly (1978) and has the form

$$R_D = \begin{cases} 0.0 & for \quad z < z_D \\ \alpha_R \{ 1 - \cos [\pi (z - z_D) / (z_T - z_D)] \} / 2 & for\ z \geq z_D \end{cases} \tag{6.4.12}$$

where z_B is the height of the bottom of the damping layer and z_T the height of the model top boundary. The depth of the damping layer $(z_T - z_B)$ depends on the type of problem being considered. In general, a layer depth 1/3 of the total domain depth or one vertical wavelength is recommended. The damping layer should be located above the part of model domain where the solution is of interest. α_R^{-1} is the e-folding time scale of damping at $z=z_T$, and a value on the order of 10 to 50 big time steps is recommended.

6.5. Grid Structure and Boundary Conditions

6.5.1. Introduction

In a regional atmospheric model, only the lower boundary is physical. The boundaries at the top and sides are usually artificial. ARPS permits the user to choose different types of boundary conditions for the lateral, top and bottom boundaries.

Five types of lateral boundary conditions are available in ARPS: rigid wall, periodic, zero normal gradient, wave-radiating open boundary, and externally specified boundary conditions. All five options can be specified independently for each lateral boundary. Three types of boundary conditions are available at the top and bottom boundaries: rigid top lid (impermeable ground), periodic, and zero-normal gradient. Wave reflection from the rigid top boundary can be suppressed by use of a Rayleigh damping layer near the top boundary (see Section 6.4.3).

To implement the boundary conditions, extra grid points are defined outside the physical boundary of the model domain. These extra points are often referred to as the "fake" points or zones. The graphical relationship between the physical domain and the boundary points is shown in Figure 6.2a for the ξ - η (x - y) cross-section and in Fig. 6.2b for the ξ – ζ (x - z) cross-section of the model domain. In the figure, the physical boundary is shown as the thick line and the physical domain (model interior domain) is shaded. The fake points outside the physical domain constitute the computational boundaries, and the locations of these boundaries vary with the variables due to grid staggering. For example, the computational boundaries of horizontal velocity u are at $\xi = -\Delta\xi$ and $\xi = L_\xi + \Delta\xi$ in the ξ direction, and at $\eta = -\Delta\eta/2$ and $\eta = L_\eta + \Delta\eta/2$ in the η direction. On this grid, second order advection and mixing terms can be readily calculated in the interior domain for all prognostic variables.

In Figure 6.2, the physical boundary is located at the grid points of the normal velocity components (*e.g.*, the physical boundary on the west side coincides with the grid points of the u-velocity). The normal velocity components are defined up to one grid interval outside the physical boundary, and all the other variables are defined up to half a grid interval outside.

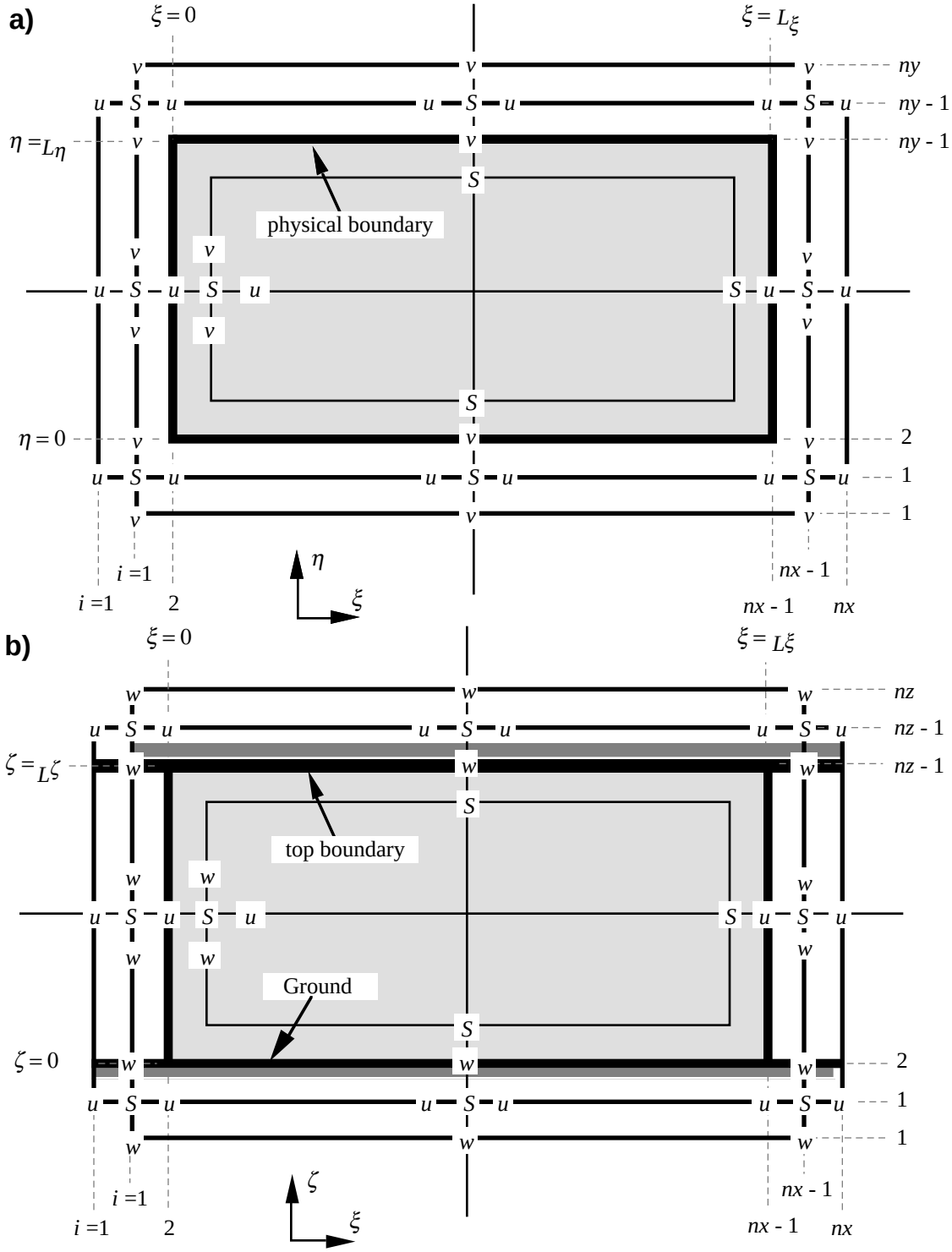

Figure 6.2. The ξ–η plane of the model grid. 6.2a shows the variable arrangement relative to the physical boundary. *S* represents the scalar variables. The layout of the grid in the ξ-ζ plane is similar (6.2b), except that η and *v* are replaced by ζ and *w*.

In ARPS code, all three dimensional arrays have the dimensions *(*1*:nx,* 1*:ny,* 1*:nz)*. For certain variables, the elements at *i*=*nx,* or *j*=*ny* or *k*=*nz* are redundant. More specifically,

- *u* is defined from *(*1*:nx,* 1*:ny*-1, 1*:nz*-1*)* in the index space, with computational boundaries at *i*=1 and *nx* in the ξ direction, at *j*=1 and *ny*-1 in the η direction, and at *k*=1 and *nz*-1 in the ζ direction.

- *v* is defined from *(*1*:nx*-1, 1*:ny,* 1*:nz*-1*)* in the index space, with computational boundaries at *i*=1 and *nx*-1 in the ξ direction, at *j*=1 and *ny* in the η direction, and at *k*=1 and *nz*-1 in the ζ direction.

- *w* is defined from *(*1*:nx*-1, 1*:ny*-1, 1*:nz)* in the index space, with computational boundaries at *i*=1 and *nx*-1 in the ξ direction, at *j*=1 and *ny*-1 in the η direction, and at *k*=1 and *nz* in the ζ direction.

- The scalars (*p*, θ, *q*, *etc.*) are defined from *(*1*:nx*-1, 1*:ny*-1, 1*:nz*-1*)* in the index space, with computational boundaries at *i*=1 and *nx*-1 in the ξ direction, at *j*=1 and *ny*-1 in the η direction, and at *k*=1 and *nz*-1 in the ζ direction.

On ARPS grid, the scalar point is located at the center of a 3-D grid cell. The normal velocity components are located on the six sides of this cell. The index range for the cells inside the physical boundary are from *i*=2 to *nx*-2, *j*=2 to *ny*-2 and *k*=2 to *nz*-2 in the three coordinate directions, respectively. These index bounds should be used if a volume integral of the entire domain is to be calculated, with the velocity components averaged to the cell centers before an integral operation.

6.5.2. Lateral boundary conditions

Five options, to be discussed below, are available for the lateral boundary condition:

1. Wall (or mirror) boundary condition;
2. Periodic boundary condition;
3. Zero-normal gradient condition;
4. Open (radiative) boundary condition;
5. Externally specified boundary condition.

a) Wall or mirror condition

For a free-slip rigid wall, a mirror type boundary condition is imposed. For illustration purposes, we consider a two dimensional case, and look at the left boundary of the ξ–ζ slab at $\xi = 0$ (Figure 6.3). The free-slip condition dictates that $w(\xi = -\Delta\xi / 2) = w(\xi = \Delta\xi / 2)$. A rigid wall requires $u(\xi = 0) = 0$. By taking a ξ-derivative of the incompressible mass continuity equation, so that $\partial[\partial u / \partial\xi + \partial w / \partial\zeta] / \partial\xi = 0$, and making use of the free-slip condition, $\partial w / \partial\xi = 0$, we have $\partial^2 u / \partial\xi^2 = 0$. From $\partial^2 u / \partial\xi^2 = 0$ and $u = 0$ at $\xi = 0$, we arrive at $u(\xi = -\Delta\xi) = - u(\xi = \Delta\xi)$, which is the mirror boundary condition.

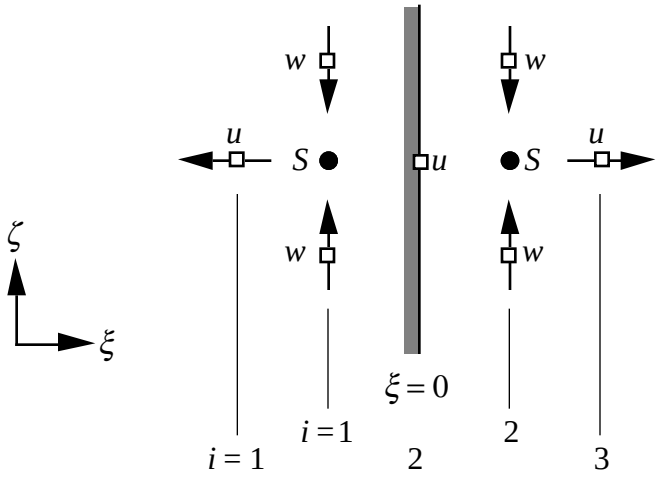

Figure 6.3. Illustration of mirror boundary condition. The flow pattern is symmetric about the solid wall located at $\xi = 0$.

Given that $u\,(\xi = 0) = 0$ and all the other variables are symmetric about the wall, the advection and mixing terms are zero at the lateral boundary. The pressure gradient across the boundary must also be zero for the normal velocity equation to be valid at the boundary. Therefore, for all scalars, the symmetric condition is applied, *i.e.* $\partial S / \partial\xi = 0$ at $\xi = 0$.

In the model, the mirror boundary condition for the lateral boundaries are implemented as follows:

At the ξ boundaries:

$u(1,j,k)$	$= -u(3,j,k)$	and $u(nx,j,k)$	$= -u(nx-2,j,k)$	for all j,k.
$v(1,j,k)$	$= v(2,j,k)$	and $v(nx-1,j,k)$	$= v(nx-2,j,k)$	for all j,k.
$W^c(1,j,k)$	$= W^c(2,j,k)$	and $W^c(nx-1,j,k)$	$= W^c(nx-2,j,k)$	for all j,k.

$$S(1,j,k) = S(2,j,k) \quad \text{and} \quad S(nx\text{-}1,j,k) = S(nx\text{-}2,j,k) \quad \text{for all } j,k. \tag{6.5.1}$$

and the η boundaries:

$$\begin{aligned}
&u(i,1,k) = u(i,2,k) && \text{and } u(i,ny\text{-}1,k) = u(i,ny\text{-}2,k) && \text{for all } i,k.\\
&v(i,1,k) = -v(i,3,k) && \text{and } v(i,ny\ ,k) = -v(i,ny\text{-}2,k) && \text{for all } i,k.\\
&W^c(i,1,k) = W^c(i,2,k) && \text{and } W^c(i,ny\text{-}1,k) = W^c(i,ny\text{-}2,k) && \text{for all } i,k.\\
&S(i,1,k) = S(i,2,k) && \text{and } S(i,ny\text{-}1,k) = S(i,ny\text{-}2,k) && \text{for all } i,k.
\end{aligned} \tag{6.5.2}$$

where S represents a scalar, *e.g.*, pressure, potential temperature or a water quantity.

For the contravariant velocity W^c, the mirror type boundary condition is applied. The Cartesian velocity w is then derived from u, v and W^c.

After these boundary values are set, the interior values can be computed by the prognostic equations when second order spacial differencing is applied. When a high order scheme is used, special boundary treatment is usually required. The normal velocity components at the physical boundaries are considered to be interior and are explicitly predicted by their equations. The predicted u at ξ=0 and L_ξ, and v at η=0 and $L_{\eta,}$ should be zero.

b) Periodic boundary condition

The periodic boundary condition assumes that the solution outside the computational domain replicates itself indefinitely. The solution at a distance d to the left of the computational domain boundary equals the solution a distance d to the left of the right boundary.

In ARPS, the periodic boundary conditions are implemented as follows:

At the ξ boundaries:

```
u(1,j,k)=u(nx-2,j,k), u(nx ,j,k)=u(3,j,k)   for all j,k.
v(1,j,k)=v(nx-2,j,k), v(nx-1,j,k)=v(2,j,k)  for all j,k.
w(1,j,k)=w(nx-2,j,k), w(nx-1,j,k)=w(2,j,k)  for all j,k.
S(1,j,k)=S(nx-2,j,k), S(nx-1,j,k)=S(2,j,k)  for all j,k.
wcont(1,j,k)=wcont(nx-2,j,k) and
wcont(nx-1,j,k)=wcont(2,j,k) for all j,k.                (6.5.3)
```

and at the η boundaries:

```
u(i,1,k)=u(i,ny-2,k), u(i,ny-1,k)=u(i,2,k)  for all i,k.
v(i,1,k)=v(i,ny-2,k), v(i,ny ,k)=v(i,3,k)   for all i,k.
w(i,1,k)=w(i,ny-2,k), w(i,ny-1,k)=w(i,2,k)  for all i,k.
S(i,1,k)=S(i,ny-2,k), S(i,ny-1,k)=S(i,2,k)  for all i,k.
wcont(i,1,k)=wcont(i,ny-2,k) and
wcont(i,ny-1,k)=wcont(i,2,k) for all i,k.                (6.5.4)
```

The periodic boundary conditions are directly applied to both *w* and W^c.

As in the case of wall boundary condition, the interior values are predicted by second order finite differencing schemes, the boundary conditions having been set. When a higher order advective scheme is used, special boundary treatment is required. The normal velocity components at the physical boundaries are considered to be interior and are explicitly predicted by their equations. The predicted *u* at $\xi=0$ should equal *u* at $\xi=L_\xi$ and *v* at $\eta=0$ equals *v at* $\eta=L_\eta$ in the periodic case.

c) Zero gradient boundary condition

For this type of boundary condition, the gradients of all variables at the lateral boundaries are set to zero. The expressions are similar to those given in (6.5.1) and (6.5.2) for the mirror boundary condition, except that all minus signs on the right hand side of the equations are changed to positive signs.

d) Wave-radiation open boundary condition

Wave radiation boundary conditions are designed to allow waves in the interior of the model domain to pass out freely through the boundary with minimal reflection. Radiation boundary conditions typically employ a simplified wave propagation equation to determine the time rate of change of the predicted variables at the lateral boundaries. Based on the study by Oliger and Sundstrom (1976) on the well-posedness of boundary conditions, the wave equation is applied only to the normal components of velocity at the boundaries in ARPS. Other variables, i.e., the components of velocity parallel to the boundary, the potential temperature and water variables are predicted on the boundary using the same prognostic equations as used in the interior. However, at the lateral boundaries, upstream advection replaces the centered advection on the boundary. The advection at the inflow boundary is set to zero, which is based on the assumption that no gradient exists in the field outside the boundary. The turbulent mixing terms at the boundary are set to

the values of the adjacent interior point. The second and fourth order computational mixing are computed in the same way as in the interior, but with the assumption that the normal gradient in the fields outside the boundary is zero.

Several variations of the radiation boundary condition are available. Orlanski (1976) proposed a type in which the prognostic equation for a variable ψ is replaced by an one dimensional wave equation

$$\frac{\partial \psi}{\partial t} + c \frac{\partial \psi}{\partial \xi} = 0 \tag{6.5.5}$$

where c is a phase speed of wave signal propagation, which is estimated locally using the same equation applied at one time step earlier and one grid point interior of the boundary. Miller and Thorpe (1981) discussed a number of variations of the original Orlanski formulation. Durran and Klemp (1983) applied a vertical average on the locally estimated c and used the averaged c in their mountain flow simulations.

Another variation of the radiation condition is to use the wave equation

$$\frac{\partial \psi}{\partial t} + (u+C) \frac{\partial \psi}{\partial \xi} = 0 \tag{6.5.6}$$

where u is the flow speed normal to the boundary, and C is a constant phase speed, representing that of the dominant wave signals. This scheme is suggested by Klemp and Wilhelmson (1978). Klemp and Wilhelmson (1978) and others (*e.g.*, Tripoli and Cotton, 1980) implemented the open boundary condition using (6.5.6) in the large time step of the split-explicit time integration system. The C is regarded as the typical internal gravity wave propagation speed. Theory and experiments (*e.g.*, Lilly, 1980; Clark, 1979) show that an over-estimation of C is better than a underestimation of the same amount. Therefore, C is usually taken as the fastest propagating gravity wave speed, a typical estimation is HN/π, where H is the domain depth and N the representative Brunt-Väisälä frequency. A constant value between 30 and 45 m/s is often chosen for storm simulations (*e.g.*, Tripoli and Cotton, 1980; Clark, 1979).

Based on many tests on the above variations of radiation boundary conditions, ARPS includes four radiation boundary condition options. These are:

rbcopt = 1: Klemp-Wilhelmson formulation with Eq. (6.5.6) applied on the small time step;

rbcopt = 2: Klemp-Wilhelmson formulation with Eq. (6.5.6) applied on the large time step;

rbcopt = 3: Orlanski formulation based on Eq. (6.5.5). With this scheme, *c* is computed on the big time step and Eq. (6.5.5) is applied on the small time step;

rbcopt = 4: Orlanski formulation with additional vertical averaging of the calculated *c* after Durran and Klemp (1983).

To illustrate the Klemp-Wilhelmson condition on the small time step (*rbcopt=1)*, Eq. (6.5.6) is applied to *u* at the *x* boundary (note: the same analysis can be performed for *v* on the *y* boundary).

The wave equation (6.5.6) applied to *u* is

$$\frac{\partial u}{\partial t} + (u + C)\frac{\partial u}{\partial x} = 0, \tag{6.5.7}$$

Equation (6.5.7) is discretized using forward-in-time and upstream-in-space difference schemes on the small time step.

For the right boundary, $C > 0$, we have

$$\frac{u_{nx}^{\tau+\Delta\tau} - u_{nx}^{\tau}}{\Delta\tau} = -(u_{nx}^{\tau} + C)\frac{u_{nx}^{\tau} - u_{nx-1}^{\tau}}{\Delta x}, \qquad \text{if } u + C > 0 \tag{6.5.8}$$

$$\frac{u_{nx}^{\tau+\Delta\tau} - u_{nx}^{\tau}}{\Delta\tau} = -\gamma\left(u_{nx}^{\tau} + C\right)\frac{\bar{u}_{nx} - u_{nx}^{\tau}}{\Delta x} = -\gamma\left|u_{nx}^{\tau} + C\right|\frac{u_{nx}^{\tau} - \bar{u}_{nx}}{\Delta x}, \qquad \text{if } u + C \le 0 \tag{6.5.9}$$

where subscript *nx* is the grid point index at the right boundary for *u.* When $u + C > 0$, upstream advection gives (6.5.8). When $u + C \le 0$, (6.5.9) is obtained by discretizing (6.5.7) using the forward-in-time, upstream-in-space difference scheme, with the assumption that *u* outside the boundary has the base-state value if $\gamma = 1$, and *u* outside the boundary equals *u* at the boundary (zero gradient) if $\gamma = 0$. For $0 < \gamma < 1$, the boundary *u* is relaxed towards the base state value using a coefficient that is proportional to $|u+C|$ at the boundary. In the original KW condition, γ is zero. In that case, the boundary value remains unchanged in time when $u + C$ is directed into the model domain.

The corresponding equations for the left boundary are:

$$\frac{u_1^{\tau+\Delta\tau} - u_1^{\tau}}{\Delta\tau} = -(u_1^{\tau} + C)\frac{u_2^{\tau} - u_1^{\tau}}{\Delta x}, \qquad \text{if } u + C < 0 \tag{6.5.10}$$

$$\frac{u_1^{\tau+\Delta\tau}-u_1^{\tau}}{\Delta\tau} = -\gamma\left(u_1^{\tau}+C\right)\frac{u_1^{\tau}-\bar{u}_1}{\Delta x} = -\gamma\left|u_1^{\tau}+C\right|\frac{u_1^{\tau}-\bar{u}_1}{\Delta x},$$

if $u+C\geq 0$. (6.5.11)

where subscript 1 is the grid point index at the left boundary for u. In the model code, γ = *rlxlbc* and $|C|$ = *c_phase*, both assigned in the input file (see Chapter 4). These calculations can be found in subroutine BKWSMLDT in file *setbdt3d.f*.

For *rbcopt* = 2, the Klemp and Wilhelmson (1978) condition is applied to the large time step. Again, the normal velocity component is predicted by a simplified wave equation. We show this for the x boundary as an example:

$$\frac{\partial u}{\partial t} + (u+C)\frac{\partial u}{\partial x} = 0 \qquad (6.5.12)$$

where C is the typical speed of internal gravity waves and is usually chosen to be the fastest outward propagating gravity wave speed in the model domain.

Equation (6.5.12) is discretized using centered-in-time and upstream-in-space difference scheme. The time differencing is consistent with that used for the model interior.

For the right boundary, $C>0$, we have

$$\frac{u_{nx}^{t+\Delta t}-u_{nx}^{t-\Delta t}}{2\Delta t} = -\left(u_{nx}^{t}+C\right)\frac{u_{nx}^{t}-u_{nx-1}^{t}}{\Delta x} \qquad \text{if } u+C>0 \qquad (6.5.13)$$

$$\frac{u_{nx}^{t+\Delta t}-u_{nx}^{t-\Delta t}}{2\Delta t} = -\gamma\left(u_{nx}^{t}+C\right)\frac{\bar{u}_{nx}-u_{nx}^{t-\Delta t}}{\Delta x} = -\gamma\left|u_{nx}^{t}+C\right|\frac{u_{nx}^{t-\Delta t}-\bar{u}_{nx}}{\Delta x}$$

if $u+C\leq 0$ (6.5.14)

where subscript *nx* is the grid point index at the right boundary for u. The spatial differencing is the same as for option one, but for time, leap-frog scheme is used here reather than the forward scheme.

For completeness, the corresponding equations for the left boundary are:

$$\frac{u_1^{t+\Delta t}-u_1^{t-\Delta t}}{2\Delta t} = -\left(u_1^{t}+C\right)\frac{u_2^{t}-u_1^{t}}{\Delta x}, \qquad \text{if } u+C<0 \qquad (6.5.15)$$

$$\frac{u_1^{t+\Delta t}-u_1^{t-\Delta t}}{2\Delta t} = -\gamma\left(u_1^{t}+C\right)\frac{u_1^{t-\Delta t}-\bar{u}_1}{\Delta x} = -\gamma\left|u_1^{t}+C\right|\frac{u_1^{t-\Delta t}-\bar{u}_1}{\Delta x},$$

if $u+C\geq 0$. (6.5.16)

where subscript 1 is the grid point index at the left boundary for *u*. In the model code, γ = *rlxlbc* and $|C|$ = *c_phase*. This part of calculations can be found in subroutine BDTU in file *setbdt3d.f*.

For the Orlanski type boundary condition (*rbcopt* = 3), *c* is determined locally and is therefore spatially and temporarily varying. The estimated phase speed $\hat{c}$ is obtained from (6.5.5) and applied to *u* and *v*. For the *u* velocity,

$$\hat{c}_\xi = [(u^{n-2}_{2jk} - u^{n}_{2jk}) / (- u^{n}_{2jk} - u^{n-2}_{2jk} + 2\, u^{n-1}_{3jk})] * \Delta\xi/\Delta t \qquad (6.5.17)$$

at the west boundary, and

$$\hat{c}_\xi = [(u^{n-2}_{nx-1jk} - u^{n}_{nx-1jk}) / (u^{n}_{nx-1jk} + u^{n-2}_{nx-1jk} - 2\, u^{n-1}_{nx-2jk})] * \Delta\xi/\Delta t \qquad (6.5.18)$$

at the east boundary.

For *v*,

$$\hat{c}_\eta = [(v^{n-2}_{i2k} - v^{n}_{i2k}) / (- v^{n}_{i2k} - v^{n-2}_{i2k} + 2\, v^{n-1}_{i3k})] * \Delta\eta/\Delta t \qquad (6.5.19)$$

at the south boundary, and

$$\hat{c}_\eta = [(v^{n-2}_{iny-1k} - v^{n}_{i\,ny-1k}) / (v^{n}_{iny-1k} + v^{n-1}_{iny-1k} - 2\, v^{n-1}_{iny-2k})] * \Delta\eta/\Delta t \qquad (6.5.20)$$

at the north boundary.

The estimated phase speed is subject to the limit of maximum Courant number of one. It is then used in Eq. (6.5.5) to calculate the time tendencies for *u* at the east and west boundaries and *v* at the north and south boundaries.

The fourth radiation boundary condition option (*rbcopt* = 4) incorporates vertical averaging on the Orlanski computed phase speeds following Durran and Klemp (1983). The outward directed phase speeds are averaged over the vertical extent of the model with the inward directed phase speed set to zero before averaging. The average phase speed is then applied to Eq. (6.5.5) to determine the time tendencies at the boundaries. This technique was found to improve the results in tests with linear mountain waves, a falling cold bubble and for gravity wave propagation cases. The mass field was better behaved compared to the Orlanski boundary condition.

All other variables except the normal velocity components are solved from their prognostic equations directly. All forcing terms in these equations can be evaluated at the boundaries without any additional assumptions, except for the normal advection and the normal mixing terms, described previously. At the boundary, zero gradient is assumed for the turbulent mixing in the normal direction. For the computational mixing, the mixed fields are assumed

to have zero gradients outside the model domain. For the advection terms, upstream differencing is used when the flow is directed into the model domain. When the flow is directed outwards, the same relaxation procedure used in (6.5.9) and (6.5.11) is applied, with an adjustable relaxation coefficient γ built into the formulation. Again, for $\gamma = 0$, zero gradient is assumed for the advected field outside the boundary, while for $\gamma = 1$, the base state value is advected in. For $0 < \gamma < 1$, the boundary value is relaxed towards the base-state value.

e) Externally specified boundary condition

In this case, the boundary values are obtained from a user-provided external data set, or from a user-specified solution. Therefore, we set

```
u(1,j,k) and u(nx ,j,k)       for all j,k,
u(i,1,k) and u(i,ny-1,k)      for all i,k,
v(i,1,k) and v(i,ny ,k)       for all i,k,
v(1,j,k) and v(nx-1,j,k)      for all j,k,
w(1,j,k) and w(nx-1,j,k)      for all j,k,
w(i,1,k) and w(i,ny-1,k)      for all i,k,
S(1,j,k) and S(nx-1,j,k)      for all j,k,
S(i,1,k) and S(i,ny-1,k)      for all i,k.
```

to externally specified values. W^c is diagnosed from *u*, *v* and *w*. Most of the time, enhanced relaxation and damping are required in a zone near the lateral boundaries, in order to reduce the inconsistencies between the model solution and the external data. The amount of relaxation is user-specified through a parameter in the input file. Additional information on the externally forced boundary option can be found in Section 8.6.

6.5.3. Top and bottom boundary conditions

The vertical cross-section of the model grid is similar to that shown for the ξ-η plane in Figure 6.2. For a corresponding figure for the ξ–ζ cross-section, one replaces η, *NY*, *v* and *j* by ζ, *NZ*, *w* and *k*.

In the vertical direction, *u*, *v* and scalars are defined from $k = 1$, $nz - 1$. The time integration is performed from $k = 2$ to $nz - 2$ and their boundary conditions are specified at $k = 1$ and $nz - 1$. *w* is defined from $k = 1$, nz and its boundary conditions are specified at $k = 1$ and nz. In the case of a rigid top lid and solid ground, *w* is also specified at $k = nz - 1$ and at $k = 2$, respectively.

ARPS assumes the model top boundary is flat, and is at height $z = \zeta = H$. The contravariant velocity W^c, defined as the component of velocity vector

normal to ζ = constant surface, vanishes at the lid. The Cartesian vertical velocity w, defined as $w = u\partial H/\partial\xi + v\partial H/\partial\eta + W^c\partial H/\partial\zeta$ also vanishes there.

Given that $w = W^c=0$ at $z = H$, the mirror free-slip boundary condition requires

$$\partial u/\partial\zeta = \partial v/\partial\zeta = \partial S/\partial\zeta = 0 \ \ at \ \ \zeta = H,$$
$$\text{and} \quad W_c\,(\zeta = H+\Delta\zeta) \ = \ - W_c\,(\zeta = H-\Delta\zeta). \tag{6.5.21}$$

In the code, they are:

```
wcont(i,j,nz-1)=0.0              for all i,j,
wcont(i,j,nz)=-wcont(i,j,nz-2)   for all i,j,
u(i,j,nz-1)=u(i,j,nz-2)          for all i,j,
v(i,j,nz-1)=v(i,j,nz-2)          for all i,j,
S(i,j,nz-1)=S(i,j,nz-2)          for all i,j.
```

The bottom boundary is at $z = h(x,y)$, where h is the terrain height. When the terrain is not flat, vertical velocity will not be zero at the ground. The terrain-following coordinate transformation used by ARPS ensures that the computational grid line ($\zeta = 0$) at the lower boundary follows the terrain.

At the non-penetrative lower boundary, the definition of W^c requires that

$$W^c = 0 \ \text{ at } \ \zeta = 0 \ \text{ or } \ z = h. \tag{6.5.22}$$

According to the definition of w, we have

$$w = u\partial h/\partial\xi + v\partial h/\partial\eta \ \ \text{ at } \ \zeta = 0 \ \text{ or } \ z = h \tag{6.5.23}$$

which can also be obtained by applying the zero normal velocity condition at the ground. The mirror type boundary condition based on mass continuity gives:

$$W^c(\zeta = -\Delta\zeta\,) \ = -W^c(\zeta + \Delta\zeta\,).$$

where $w(\zeta = -\Delta\zeta\,)$ can be derived from u, v and W^c. In ARPS, these conditions appear as:

```
u (i,j,1) = u(i,j,2),
v (i,j,1) = v(i,j,2),
wcont(i,j,2)= 0 ,
w (i,j,2) = u∂h/∂x + v∂h/∂h,
```

```
S (i,j,1) = S(i,j,2).
```

Here, *S* stands for all scalar variables except for *p'*. For *p'*, an extrapolated boundary condition is used: *p'* (i, j, 1) = -*p'* (i, j, 3) + 2*p'* (i, j, 2).

In the vertical direction, the time integration is carried out from $k = 2$, $nz - 2$ for *u*, *v*, and all scalars, and from $k = 3$ to $nz - 2$ for *w*..

Apart from the rigid top and bottom boundary conditions, periodic and zero gradient boundary conditions are also available at the vertical boundaries, *except when the vertically implicit* w *and* p *solver is used*. The implementations are straightforward.

6.5.4. The base state boundary conditions

The base state density, temperature, pressure and water vapor mixing ratio at the lateral boundaries are initialized using the same method as the interior points. Zero vertical gradients are assumed for $\bar{\theta}$ and $\bar{q}_v$, and the hydrostatic relation is used to obtain $\bar{p}$ and other thermodynamic variables at the top and bottom boundaries.

6.6. Warm Rain Microphysics Parameterization

The Kessler warm rain microphysics parameterization considers three categories of water; water vapor, cloud water and rain water. Each of the liquid water forms is implicitly characterized by a droplet distribution. Small cloud droplets are first formed when the air becomes saturated and condensation occurs. If the cloud water mixing ratio exceeds a threshold value, raindrops are formed by auto-conversion from the cloud droplets. The raindrops then collect smaller cloud droplets by accretion as they fall at their terminal speed. If cloud droplets enter unsaturated air they evaporate until either the air is saturated or until the droplets are exhausted. Raindrops also evaporate in a subsaturated environment at a rate depending on their concentration and the saturation deficit. When the ice phase is included, many more processes will be involved. These processes are discussed later in Section 6.7.

This section describes the Kessler warm rain microphysics parameterization scheme used in ARPS 4.0. It is based on the descriptions given by Klemp and Wilhelmson (1978) and Soong and Ogura (1973).

6.6.1. Autoconversion rate of cloud water to rain water

The rate of autoconversion of cloud to rain water is approximated by the simple relation

$$A_r = C_{ar} (q_c - q_{ccrit}) \tag{6.6.1}$$

where A_r is the autoconversion rate of cloud water to rain water in kg kg^{-1}s^{-1}, q_c is the cloud water mixing ratio in kg kg^{-1}, $q_{c\ crit}$ = 1 x 10^{-3} kg kg^{-1} is the cloud water mixing ratio threshold, and C_{ar} = 1 x 10^{-3} s^{-1} is the autoconversion rate.

6.6.2. Accretion (collection)of cloud water by rainwater

The rate of accretion of cloud water by rain water is approximated by:

$$C_r = C_{cr}\, q_c\, q_r^{0.875} \tag{6.6.2}$$

where C_r is the accretion rate of cloud water by rain water in kg kg^{-1}s^{-1}, q_r is the rain water mixing ratio in kg kg^{-1}, and C_{cr} = 2.2 s^{-1}.

6.6.3. Terminal velocity of rainwater

The terminal fall velocity for the averaged-sized raindrops is

$$V_{tr} = 36.34\ (0.001\ \bar{\rho}\ q_r)^{0.1364}\ (\rho_o/\bar{\rho})^{0.5} \tag{6.6.3}$$

where V_{tr} is the terminal velocity of air in m s^{-1}, $\bar{\rho}$ is the base state density in kg m^{-3}, ρ_o = 1.225 kg m^{-3} is the reference density.

6.6.4. Rainwater evaporation rate

The evaporation rateof raindrops is defined as

$$E_r = \frac{1}{\bar{\rho}} \frac{C\,[\,1 - q_v / q_{vs}]\,[\,\bar{\rho}\ q_r\,]^{0.525}}{2.030\text{x}10^4 + 9.584\text{x}10^6 / [\,q_{vs}\,\bar{\rho}\,]} \tag{6.6.4}$$

where E_r is the evaporation rate in kg kg^{-1}s^{-1}, q_v is the water vapor mixing ratio in kg kg^{-1}, p is the pressure in Pa. Note that all over-barred variables are functions of z only. The ventilation coefficient, C, is given by

$$C = 1.6 + 30.3922\ (\bar{\rho}\, q_r)^{0.2046} \quad . \tag{6.6.5}$$

The evaporation rate is used only when the air is unsaturated.

6.6.5. Saturation adjustment

The saturation adjustment scheme computes the amount of water vapor converted to cloud water if super-saturation exists *($q_v > q_{vs}$)*, or the amount of cloud water evaporated if sub-saturation exists *($q_v < q_{vs}$)*. Here q_{vs} is saturation mixing ratio calculated from Teten's formula (6.3.19). The amount of adjustment to q_v is given by

$$\delta q_{vs} = \frac{-\left[q_v^* - q_{vs}^*\right]}{1 + \dfrac{a_w(273.15 - b_w)\, q_{vs}^* L_v / C_p}{\left[T^* - b_w\right]^2}} \tag{6.6.6}$$

with δq_{vs} subjected to the following test,

$$\delta q_{vs} = min\ [\ \delta q_{vs},\ q_c\ ]. \tag{6.6.7}$$

Here the asterisked variables have been updated for advection, diffusion, filtering, and other forcing processes, and δq_{vs} is the amount of cloud mixing ratio in kg kg^{-1} created by condensation (if negative) or evaporation (if positive).

The adjustment to the potential temperature corresponding to the change in q_v is

$$\delta\theta' = -\ \bar{\Gamma}\, \delta q_{vs}. \tag{6.6.8}$$

where $\bar{\Gamma}$ is defined as

$$\bar{\Gamma} = L_v / (\bar{\Pi} C_p) \tag{6.6.9}$$

where L_v is the latent heat of evaporation defined by:

$$L_v = 2{,}500{,}780.0\ (273.15\bar{T}^{-1})^{(0.167 + 3.67x10^{-4}\bar{T})} \quad . \tag{6.6.10}$$

The temperature has units of °K, and L_v has units of J kg^{-1}.

$\bar{\Pi}$ is the Exner function (or the non-dimensional pressure) given by:

$$\bar{\Pi} = (\bar{p} / p_o)^{R_d / C_p} \tag{6.6.11}$$

where R_d =286.04 J /(kg °K) is the gas constant for dry air, and C_p =1004. J / (kg °K) is the specific heat for dry air. P_o = 1000 mb is a constant reference pressure.

6.6.6. Differencing the microphysics scheme

The adjusted values for θ', q_v, q_c, and q_r are obtained from:

$$\theta'^{n+1} = \theta'^{*n+1} - \bar{\Gamma}(\delta q_{vs} + 2\,\Delta t\, E_r)$$
$$q_v^{n+1} = q_v^{*n+1} + \delta q_{vs} + 2\,\Delta t\, E_r$$
$$q_c^{n+1} = q_c^{*n+1} - \delta q_{vs} - 2\,\Delta t\,(A_r + C_r)$$
$$q_r^{n+1} = q_r^{*n+1} + 2\Delta t[A_r + C_r - E_r] \tag{6.6.12}$$

where Δt is the integration time step. The last term on the right hand side of the rain water equation is the fallout term.

6.6.7. Other adjustments

In ARPS, negative water quantities produced by advection and by the vertical flux terms associated with rainwater fallout are not adjusted. Rather, the negative values are set to zero and only the positive values are used in the microphysical calculations. Since both positive and negative values are involved in the advection and mixing processes, the total water content is conserved apart from the rainwater fallout. In future versions of ARPS, positive definite schemes will be used for scalar advection, so that negative values will not be generated.

6.7. Microphysics Rate Equations

In ARPS, the ice microphysics package is based on a code developed by Tao and Simpson (1993). It includes the Kessler warm rain microphysics and three-category ice-phase (cloud ice, snow and hail / graupel) parameterization schemes (Lin *et al.*, 1983). The particle size distribution functions for rain (q_r), snow (q_s) and graupel / hail (q_g), are assumed to be of the form

$$N(D) = N_0 \exp(-\lambda D) \tag{6.7.1}$$

where D is the drop diameter and $N(D)$ the number of drops of diameter between D and $D + \delta D$ in unit volume of space, N_0, the intercept parameter, is the value of $N(D)$ for $D = 0$, and

$$\lambda = \left(\frac{\pi \rho_x N_0}{\rho\, q_x} \right)^{0.25} \tag{6.7.2}$$

is the slope of the particle size distribution in which ρ_x and q_x is density and mixing ratio of the hydrometeors, respectively. The typical intercept parameters used for rain, snow and graupel (hail) are 0.08 cm^{-4}, 0.04 cm^{-4}, and 0.04 cm^{-4} (0.0004 cm^{-4}), respectively. The density for rain, snow and graupel (hail) are 1 g cm^{-3}, 0.1 g cm^{-3}, and 0.4 g cm^{-3} (0.917 g cm^{-3}), respectively. The cloud ice has a single size (mono-disperse) where its diameter and density are assumed to be 2×10^{-3} cm and 0.917 g cm^{-3}, respectively.

The conservation equations for cloud water (q_c), rain (q_r), cloud ice (q_i), snow (q_s) and graupel / hail (q_g) have the form introduced in Eq.(6.2.27). In the following equation, the terms describing the rate processes correspond to Figure 6.3 and Table 6.1, in which the various processes are described.

$$S_{q_c} = \bar{\rho}\left(c - e_c\right) - T_{qc} + D_{qc} \tag{6.7.3}$$

$$S_{q_r} = \bar{\rho}\left(-e_r + m - f\right) - T_{qr} + D_{qr} \tag{6.7.4}$$

$$S_{q_c} = \bar{\rho}\left(d_i - s_i\right) - T_{qi} + D_{qi} \tag{6.7.5}$$

$$S_{q_s} = \bar{\rho}\left(d_s - s_s - m_s + f_s\right) - T_{qs} + D_{qs} \tag{6.7.6}$$

$$S_{q_c} = \bar{\rho}\left(d_g - s_g - m_g + f_g\right) - T_{qg} + D_{qg} \tag{6.7.7}$$

where $m = m_s + m_g$, and $f = f_s + f_g$ (Lin et *al.*, 1983). The symbols *c, e, f, m, d* and *s* stand for the rates of condensation, evaporation of droplets, freezing of raindrops, melting of snow and graupel, deposition of ice particles, and sublimation of ice particles, respectively. The terms D_{qc}, $D_{qr,}$ D_{qi}, D_{qs}, and D_{qg} are subgrid-scale diffusion terms for q_c, q_r, q_i and q_g, respectively. The terms T_{qc}, T_{qr}, T_{qi}, T_{qs} and T_{qg} are microphysical transfer rates between hydrometeor species, and their sum is zero. They are defined as:

$$T_{qc} = -\left(P_{sacw} + P_{raut} + P_{racw} + P_{sfw} + D_{gacw} + Q_{sacw} + Q_{gacw}\right) - P_{i\,\mathrm{hom}} + P_{imlt} - P_{idw} \tag{6.7.8}$$

$$T_{qi} = -\left(P_{saut} + P_{saci} + P_{raci} + P_{sfi} + D_{gaci} + W_{gaci}\right) + P_{i\,\mathrm{hom}} - P_{imlt} + P_{idw} \tag{6.7.9}$$

$$T_{qr} = Q_{sacw} + P_{raut} + P_{racw} + Q_{gacw} - \left(P_{iacr} + D_{gacr} + W_{gacr} + P_{sacr} + P_{gfr}\right) \tag{6.7.10}$$

$$T_{qs} = P_{saut} + P_{saci} + P_{sacw} + P_{sfw} + P_{sfi} + \delta_3 P_{raci} + \delta_3 P_{iacr} + \delta_2 P_{sacr} - \left[P_{gacs} + D_{gacs} + W_{gacs} + P_{gaut} + \left(1 - \delta_2\right)P_{racs}\right] \tag{6.7.11}$$

$$T_{qg} = \left(1 - \delta_3\right)P_{raci} + D_{gaci} + W_{gaci} + D_{gacw} + \left(1 - \delta_3\right)P_{iacr} + P_{gacs} + D_{gacs} + W_{gacs} + P_{gaut} + \left(1 - \delta_2\right)P_{racs} + D_{gacr} + W_{gacr} + \left(1 - \delta_2\right)P_{sacr} + P_{gfr} \tag{6.7.12}$$

where

$$W_{gacr} = P_{wet} - D_{gacw} - W_{gaci} - W_{gacs}.$$

For T > 273.16°K,

$$P_{saut} = P_{saci} = P_{sacw} = P_{raci} = P_{iacr} = P_{sfi} = P_{sfw} = D_{gacs} = W_{gacs} = D_{gacw} = D_{gacr} = P_{gwet} = P_{racs} = P_{sacr} = P_{gfr} = P_{gaut} = P_{imlt} = 0 \tag{6.7.13}$$

For T < 273.16°K,

$$Q_{sacw} = Q_{gacw} = P_{gacs} = P_{idw} = P_{i\,\mathrm{hom}} = 0. \tag{6.7.14}$$

In the preceeding equations, $\delta_2 = 1$ for a grid box in which q_r and $q_s < 1 \times 10^{-4}$ g g^{-1}, and otherwise is defined as zero. $\delta_3 = 1$ for a grid box in which $q_r < 1 \times 10^{-4}$ g g^{-1}, and otherwise is defined as zero (see Lin *et al.*, 1983). D_{gaci}, D_{gacr} and D_{gacs} (W_{gaci}, W_{gacr} and W_{gacs}) are production rates for dry (wet) growth of hail. A schematic diagram of microphysical processes is shown in Figure 6.4. The explicit formulation of these hydrometeor transformations can be found in Lin *et al.* (1983).

A saturation adjustment scheme that calculates the amount of condensation (and/or deposition) necessary to remove any supersaturated vapor, or the amount of evaporation (and/or sublimation) necessary to remove any subsaturation in the presence of cloud water (cloud ice) is needed for a non-hydrostatic cloud model. A relaxation technique (*e.g.*, Newton-Raphson method) is used to iteratively balance the heat exchange and change of phase of water substance (Tao, *et al.*, 1989). Initiation of cloud ice (P_{int}) and depositional growth of cloud ice (P_{depi}) discussed in Rutledge and Hobbs (1984) is used to initiate the cloud ice in a saturated environment. This procedure weighs the saturation mixing ratio in favor of ice at levels above the freezing level 0°C. This adjustment scheme will almost guarantee that the cloudy region (defined as the area which contains cloud water and/or cloud ice) is always saturated (100% relative humidity). This permits subsaturated downdrafts with rain and hail/graupel particles but not cloud-sized particles.

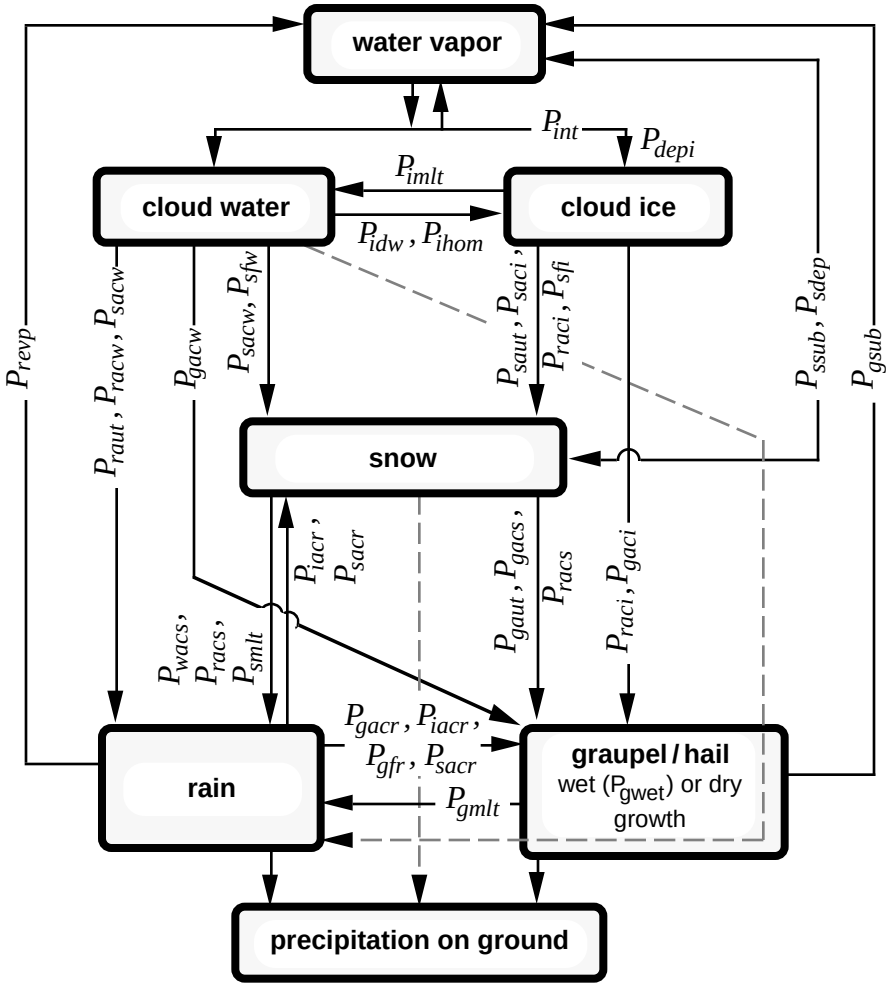

Figure 6.4. Cloud microphysical processes considered in the ice microphysics parameterization scheme (after Lin *et al.*, 1983).

Table 6.1. Definition of symbols used in microphysics parameterization

Symbol	Definition
P_{depi}	Depositional growth of cloud ice.
P_{int}	Initiation of cloud ice.
P_{imlt}	Melting of cloud ice to cloud water.
P_{idw}	Depositional growth of cloud ice at the expense of cloud water.
$P_{i\,\text{hom}}$	Homogeneous freezing of cloud water to cloud ice.
P_{iacr}	Accretion of rain by cloud ice; producing snow or graupel depending on the amount of rain.
P_{raci}	Accretion of cloud ice by rain; producing snow or graupel depending on the amount of rain.
P_{raut}	Autoconversion of cloud water to rain.
P_{racw}	Accretion of cloud water by rain.
$P_{revp(e_r)}$	Evaporation of rain.
P_{racs}	Accretion of snow by rain; producing graupel if rain or snow exceeds threshold and $T < 273.16$ or rain if $T > 273.16$.
$P(Q)_{sacw}$	Accretion of cloud water by snow; producing snow (P_{sacw}) if $T < 273.16$ or rain (Q_{sacw}) if $T > 273.16$.
P_{sacr}	Accretion of rain by snow; producing graupel if rain or snow exceeds threshold; if not, produces snow.
P_{saci}	Accretion of cloud ice by snow.
P_{saut}	Autoconversion (aggregation) of cloud ice to snow.
P_{sfw}	Bergeron process (deposition and riming) - transfer of cloud water to snow.
P_{sfi}	Bergeron process embryos (cloud ice) used to calculate transfer rate of cloud water to snow (P_{sfw}).
$P_{sdep(d_s)}$	Deposition growth of snow.
$P_{ssub(S_s)}$	Sublimation of snow.
$P_{smlt(m_s)}$	Melting of snow to rain, $T > 273.16$.
P_{wacs}	Accretion of snow by cloud water to form rain, $T > 273.16$.
P_{gaut}	Autoconversion (aggregation) of snow to graupel.
$P_{gfr(f_g)}$	Probabilistic freezing (B_{igg}) of rain to graupel.
$D(Q)_{gacw}$	Accretion of cloud water by graupel.
$D(W)_{gaci}$	Accretion of cloud ice by graupel.
$D(W)_{gacr}$	Accretion of rain by graupel.

$P_{gsub(s_g)}$	Sublimation of graupel.
$P_{gmlt(m_g)}$	Melting of graupel to form rain, T > 273.16. (In this regime, Q_{gacw} is assumed to be shed as rain.)
P_{gwet}	Wet growth of graupel; may involve W_{gacs} and W_{gaci} and must include D_{gacw} or W_{gacr}, or both. The amount of W_{gacw} which is not able to freeze is shed to rain.

6.8. PBL Depth Calculation

The planetary boundary layer (PBL) processes and the dispersion of atmospheric pollutants are limited by the PBL depth. Therefore, the prediction of the PBL depth is of great practical concern. In addition, the development of certain convective systems(*e.g.*, dryline-forced thunderstorms) is sensitive to the PBL depth . ARPS predicts the time evolution of PBL depth in response to the surface heat fluxes. ARPS will make use of the computed PBL depth to model certain physical processes in future versions of ARPS.

ARPS employs a rate equation that describes the development of the planetary boundary layer (PBL) depth as a function of time, for stable or unstable conditions. There are 4 options for *pblopt*, a parameter in the input file:

$$pblopt = \begin{cases} 0, \text{ do not compute PBL depth} \\ 1, \text{ user specified initial depth } h_0 \\ 2, \ h_0 = u_* / f \text{ in which } f \text{ is the Coriolis parameter,} \\ \quad \text{and } u_* \text{ is the frictional velocity.} \\ 3, \text{ use } \theta \text{ sounding to estimate } h_0 \end{cases}$$

Once the initial depth (h_o) is given, the time-dependent PBL depth can be calculated according to the bulk Richardson number (stability) at the top of PBL:

$$Ri_b = \frac{g}{\theta_0} \frac{(\theta_h - \theta_s)h}{U_h^2},$$

where U_h and θ_h represent the wind speed and potential temperature at the top of the PBL, and θ_0 and θ_s are the reference and the surface potential temperatures.

6.8.1. Stable boundary layer

For $Ri_b > 0$, the rate equation similar to that discussed in Nieuwstadt and Tennekes (1981) is used to predict the PBL depth. That is,

$$\frac{dh}{dt} = T^{-1}(h_e - h),$$

where

the time scale $T = -\frac{3}{4}\frac{(\theta_h - \theta_s)}{\partial\theta_s/\partial t}$,

the equilibrium height $h_e = 0.15\ \theta_0 \frac{fU_h^2 \sin\alpha\cos\alpha}{g\left|\partial\theta_s/\partial t\right|}$,

the angle between the wind at the PBL top and the surface wind $\alpha = \tan^{-1}(u_h/v_h) - \tan^{-1}(u_s/v_s)$.

Note that when the absolute value of $\partial\theta_s/\partial t$ is too small, the PBL depth will be approximated by

$$h = u_*^2/(fG\sin\alpha).$$

6.8.2. Unstable boundary layer

For $Ri_b < 0$, the rate equation from Gryning and Batchvarova (1990) is used to predict the development of the PBL depth. Let the vertical heat flux at the surface be denoted by $(\overline{w'\theta'})_s$, and the Obukhov length by

$$L = -\frac{u_*^3\theta}{\kappa g(\overline{w'\theta'})_s},$$

then the PBL depth can be predicted according to

$$\left(\frac{h^2}{(1+2A)h - 2B\kappa L}\right)\frac{dh}{dt} = \frac{(\overline{w'\theta'})_s}{(\partial\theta/\partial z)_h},$$

where A = 0.2, B = 2.5, and κ is the von Karman constant. Following Tennekes (1973), *dh/dz* is limited to $0.2[0.2gh(\overline{w'\theta'})_s/\theta]^{1/3}$.

6.9. Parameterization of the Surface Fluxes

6.9.1. Surface flux calculations

Numerical weather prediction is often sensitive to surface fluxes of heat, momentum, and moisture. A stability and roughness-length dependent surface flux model is available in ARPS using a modified Businger formulation (Businger, *et. al.*, 1971). An analytical procedure, instead of the commonly used iteration method, is used in the flux calculations for a much improved efficiency (Byun, 1990). Businger's formulation was further modified so that the results are more realistic for highly stable or highly unstable environments (Deardorff, 1972b). Options for (constant) drag coefficients are also available (options *sfcphy* = 1 and 3).

The surface fluxes enter the model as the lower boundary conditions for the momentum stresses [τ_{13} and τ_{23} in (Eq. 6.3.1)], turbulent heat flux [H_3 in Eq. (6.3.5) for θ'] and turbulent moisture flux [H_3 in Eq. (6.3.5) for q_v] at the ground surface.

The surface momentum fluxes are defined as

$$-\tau_{13}\Big|_{surface} = -\left[\bar{\rho}\,\overline{u'w'}\right]_{surface} = \bar{\rho}\,C_{dm}\max(V,V_{\min})\,u \tag{6.9.1}$$

$$-\tau_{23}\Big|_{surface} = -\left[\bar{\rho}\,\overline{v'w'}\right]_{surface} = \bar{\rho}\,C_{dm}\max(V,V_{\min})\,v \tag{6.9.2}$$

where u and v are the horizontal velocity components evaluated at the lowest grid level above the earth's surface and $V \equiv \sqrt{u^2+v^2}$ is the wind speed at the same level. V_{min} is the lower limit of V, and is included to avoid zero fluxes at calm wind condition. V_{min} is specified by the user in the input file.

The surface sensible heat flux is defined as

$$-H_3\Big|_{surface} = -\left[\bar{\rho}\,\overline{w'\theta}\right]_{surface} = \bar{\rho}\,C_{dh}\max(V,V_{\min})\left(\theta - \theta_s\right) \tag{6.9.3}$$

where θ is the potential temperature at the first grid level above the earth's surface and θ_s is the ground temperature that is either user-specified or predicted by the surface energy budget equations. The drag and exchange coefficients C_{dm} and C_{dh} can be either user-specified or computed diagnostically as described below.

When vegetation is not considered, the moisture flux at the surface is:

$$-H_3\big|_{surface} = -\left[\bar{\rho}\,\overline{w'q'_v}\right]_{surface} = \bar{\rho}\,C_{dq}\max(V,V_{\min})\left(q_v - q_{vs}\right) \tag{6.9.4}$$

where q_v is the water vapor mixing ratio at the first grid level above the ground and q_{vs} is the ground level water vapor mixing ratio, which can be user-specified or predicted by the surface energy budget equations. C_{dq} is the bulk aerodynamic coefficient for the moisture flux and is often equal to C_{dh}. When vegetation is considered, the surface moisture flux is given by Eqs. (6.10.21)-(6.10.32).

6.9.2. Surface fluxes over land

The surface roughness over the ocean is a function of surface conditions, while surface roughness over land is independent of the surface wind.

One of the practical stability parameters is the bulk Richardson number:

$$Ri_b = \frac{g}{\theta_0}\frac{\Delta\theta\left(z-z_0\right)}{U^2}, \tag{6.9.5}$$

where z is the height of the surface layer, z_0 is the surface roughness length, $\Delta\theta = \theta_1 - \theta_s$, and θ_0, θ_s and θ_1 are the base-state, surface and first model level potential temperatures, respectively. The environment is unstable, neutral or stable if $Ri_b < 0$, $Ri_b = 0$ or $Ri_b > 0$, respectively.

Let θ_* be the temperature scale representing the surface heat flux $\overline{w'\theta_s'}$ divided by the frictional velocity u_*. According to the Monin-Obukhov (1954) similarity theory,

$$u_* = C_u\,U, \text{ with } C_u = \frac{k}{\ln\left(\frac{z}{z_0}\right) - \psi_m\left(\frac{z}{L}, \frac{z_0}{L}\right)} \tag{6.9.6}$$

$$\theta_* = C_\theta\,\Delta\theta, \text{ with } C_\theta = \frac{k}{Pr_0\left(\ln\left(\frac{z}{z_0}\right) - \psi_h\left(\frac{z}{L}, \frac{z_0}{L}\right)\right)} \tag{6.9.7}$$

where k is the von Karman constant, and Pr_0 is the Prandtl number.

We note the following relationships for the drag and exchange coefficients:

$$C_{dm} = C_u^2 = \frac{u_*^2}{U^2}, \tag{6.9.8}$$

and

$$C_{dh} = C_\theta C_u = \frac{u_* \theta_*}{U \Delta\theta}. \tag{6.9.9}$$

To obtain C_{dm} and C_{dh}, our next task is to compute C_u and C_θ. We define the functional form of ψ_m and ψ_h that depends on the stability as follows.

a) Unstable condition

For unstable conditions, we have (Byun, 1990)

$$\psi_m = 2\ln\left(\frac{1+\chi}{1+\chi_0}\right) + \ln\left(\frac{1+\chi^2}{1+\chi_0^2}\right) - 2\tan^{-1}\chi + 2\tan^{-1}\chi_0 \tag{6.9.10}$$

and

$$\psi_h = 2\ln\left(\frac{1+\eta}{1+\eta_0}\right), \tag{6.9.11}$$

where

$$\chi_0 = (1-\gamma_m\zeta_0)^{1/4}, \tag{6.9.12}$$

$$\chi = (1-\gamma_m\zeta)^{1/4}, \tag{6.9.13}$$

$$\eta_0 = (1-\gamma_h\zeta_0)^{1/2}, \tag{6.9.14}$$

$$\eta = (1-\gamma_h\zeta)^{1/2} \tag{6.9.15}$$

with $\zeta_0 = z_0/L$, $\zeta = z/L$, z_0 is the roughness length, and $\gamma_m = 15$ and $\gamma_h = 9$ are specified constants. The length scale ζ (and $\zeta_0 = (z_0/z)\zeta$) is computed by the following formulation that is similar to one used in Byun (1990). When $Q_b^3 - P_b^2 \geq 0$,

$$\zeta = \frac{z(z-z_T)\left[\ln(z/z_0)\right]^2}{(z-z_0)^2 \ln(z/z_T)}\left[-2\sqrt{Q_b}\cos(\theta_b\ 3) + \frac{1}{3\gamma_m}\right], \tag{6.9.16}$$

and when $Q_b^3 - P_b^2 < 0$,

$$\zeta = \frac{z(z - z_T)\left[\ln(z/z_0)\right]^2}{(z - z_0)^2 \ln(z/z_T)} \left[-\left(T_b + \frac{Q_b}{T_b} \right) + \frac{1}{3\gamma_m} \right], \tag{6.9.17}$$

where

$$Q_b = (\frac{1}{\gamma_m^2} + 3\, s_b^2\, \frac{\gamma_h}{\gamma_m})/9 \tag{6.9.18}$$

$$\theta_b = \cos^{-1}[P_b/\sqrt{Q_b^3}\,] \tag{6.9.19}$$

$$s_b = \frac{Ri_b}{Pr_0} \tag{6.9.20}$$

$$T_b = (\sqrt{P_b^2 - Q_b^3} + |P_b|\,)^{1/3} \tag{6.9.21}$$

$$P_b = \left[\frac{-2}{\gamma_m^3} + \frac{9}{\gamma_m}(-\frac{\gamma_h}{\gamma_m} + 3)s_b^2\right]/54. \tag{6.9.22}$$

For a given Ri_b, ζ, ψ_m, ψ_h, C_u and C_θ can be computed by the above formulations.

b) Neutral condition

For the case of neutral stability, $(C_u)_{\text{neu}}$ and $(C_\theta)_{\text{neu}}$ are calculated with an extremely small negative Ri_b, and these require the use of the above equations for the unstable case.

c) Free convection condition

According to Deardorff (1972b), for free convection (highly unstable case),

$$C_u = \min\left(C_u, 2(C_u)_{\text{neu}}\right), \tag{6.9.23}$$

$$C_\theta = \min\left(C_\theta, 3.333(C_\theta)_{\text{neu}}\right) \tag{6.9.24}$$

and the exchange coefficient C_{dh} is limited by

$$C_{dh} = \min\left(C_u C_\theta, \frac{0.0019\left(\theta_s - \theta_1\right)^{\frac{1}{3}}}{U} \right). \tag{6.9.25}$$

d) Stable condition

Similar to Deardorff (1972b), for the stable case,

$$C_u = \left(C_u\right)_{\text{neu}} \left(1 - \frac{Ri_b}{Ri_c}\right), \tag{6.9.26}$$

$$C_\theta = \left(C_\theta\right)_{\text{neu}} \left(1 - \frac{Ri_b}{Ri_c}\right), \tag{6.9.27}$$

where Ri_c is a critical bulk Richardson number, and set to 3.05. For practical reasons, Ri_b in the foregoing equations is limited by

$$Ri_b = \min\left(Ri_b, 0.25 Ri_c\right). \tag{6.9.28}$$

6.9.3. Surface fluxes over ocean

Over the ocean (sea) surface, the surface roughness lengths are related to the surface wind speed. The momentum and thermal roughness lengths are computed by

$$z_0 = z \exp\left(- \frac{k}{\sqrt{c_1}} \right), \tag{6.9.29}$$

$$z_T = z \exp\left(- \frac{k\sqrt{c_1}}{Pr_0\, c_2} \right), \tag{6.9.30}$$

with $c_1 = \left(0.4 + 0.079U\right) \times 10^{-3}$ and $c_2 = 1.1 \times 10^{-3}$ (Anderson, 1993).

The bulk Richardson number for this case is given by

$$Ri_b = \frac{g}{\theta_0}\frac{\Delta\theta\left(z-z_0\right)^2}{U^2\left(z-z_T\right)}. \tag{6.9.31}$$

The same procedure as in Section 6.9.2a is used to compute surface momentum and heat fluxes over sea.

6.9.4. Linear distribution of surface fluxes in mixing layer

It is found often that subgrid scale turbulent mixing and resolved scale eddies are not effective in transporting surface momentum, heat and moisture fluxes upwards so as to develop a well-mixed boundary layer. ARPS provides an option to linearly distribute the surface fluxes calculated according to Eqs.(6.9.1)-(6.9.4) in a specified or predicted mixing layer (PBL) depth. The linearly distribution occurs when the PBL is convectively unstable.

With the linear distribution option, the vertical turbulent momentum fluxes (stresses) τ_{13} and τ_{23}, and the vertical turbulent heat and moisture fluxes H_3 in the unstable boundary layer are replaced by a function that decreases linearly from their respective surface values calculated according to Eqs.(6.9.1)-(6.9.4) to zero at the top of the boundary layer. This distribution is neccessary for applications such as land-sea breeze simulations and is similar to the treatment in Blackadar PBL parameterization scheme (Zhang and Anthes, 1982). A more accurate treatment is been investigated.

6.10. Land-Surface Energy Budget and Soil-Vegetation Model

6.10.1. Land-Surface Energy and Moisture Budgets

This model is based on the soil-vegetation model developed by Noilhan and Planton (1989) and Pleim and Xiu (1995). It is designed to simulate the essential processes involved in surface-atmosphere interactions with the minimal amount of computation time and the fewest parameters and complexities (Wong *et al.,* 1994). At present, only snow-free and non-frozen soils are considered. It requires the horizontal distribution of soil texture at the land-surface. Data of surface characteristics are discussed in Section 8.3.

The model is based on five prognostic equations:

$$\frac{\partial T_s}{\partial t} = C_T\left(R_n - H - LE\right) - \frac{2\pi}{\tau}\left(T_s - T_2\right) \tag{6.10.1}$$

$$\frac{\partial T_2}{\partial t} = \frac{1}{\tau}\left(T_s - T_2\right) \tag{6.10.2}$$

$$\frac{\partial W_g}{\partial t} = \frac{C_1}{\rho_w d_1}\left(P_g - E_g\right) - \frac{C_2}{\tau}\left(W_g - W_{geq}\right) \tag{6.10.3}$$

$$\frac{\partial W_2}{\partial t} = \frac{1}{\rho_w d_2}\left(P_g - E_g - E_{tr}\right) \tag{6.10.4}$$

$$\frac{\partial W_r}{\partial t} = veg\ P - E_r \tag{6.10.5}$$

The meaning of each of the symbols used in this section are given in Table 6.2. Eq. (6.10.1) shows that the time rate of change in soil surface temperature is the residual of the surface energy balance between net radiation R_n, surface sensible heat flux H, latent heat flux LE and T_s - T_2. The soil heat transfer. Eq. (6.10.3) shows that the time rate of change in volumetric soil moisture near the soil surface results from the residual of the precipitation rate at the ground, and the evaporation rate from the ground, and the transfer of surface soil moisture with deep soil layer moisture. Eqs. (6.10.2) and (6.10.4) describe the heat and moisture budget in deep soil. Eq. (6.10.5) predicts the time rate of change of water W_r in the canopy. The functional forms of various terms in the above set of equations are discussed as follows.

6.10.2. Radiation-soil-vegetation model

a) Thermal coefficients

The thermal coefficient C_T in (6.10.1) can be written as

$$C_T = \frac{1}{\frac{1 - veg}{C_G} + \frac{veg}{C_V}} \tag{6.10.6}$$

in which *veg* is the fractional coverage of vegetation, and the thermal coefficient of vegetation is

$$C_V = 10^{-3}\ \ \mathrm{Km^2 J^{-1}} \tag{6.10.7}$$

and the thermal coefficient of bare soil is $C_G = C_{Gsat}\left(\frac{W_{sat}}{W_2}\right)^{b/(2\ln 10)}$. (6.10.8)

b) Radiation flux

For surface heat balance, net radiative flux in (6.10.1) is given by (Wong *et al.*, 1983)

$$R_n = R_{sw}\left(1-\alpha\right) - \varepsilon_g \sigma T_s^4 + \varepsilon_a \sigma T_a^4 \tag{6.10.9}$$

in which ε_g is the emissivity of the earth's surface, $\varepsilon_a = 0.725$ is the emissivity of the air, $\sigma = 5.67\times10^{-8}\,\mathrm{Wm^{-2}K^{-4}}$ is the Stefan-Boltzman constant, and T_a is the air temperature at an atmospheric level. The total albedo is $\alpha = \alpha_s + \alpha_z$, where α_s is the albedo at polar zenith and α_z the zenith angle adjustment to α. The zenith angle adjustment is given by

$$\alpha_z = 0.01\left[\exp\left(0.003286 Z^{1.5}\right) - 1\right]$$

where Z is the solar zenith angle in radians and the minimum albedo with Z = 0 is

$$\alpha_s = \begin{cases} 0.31 - 0.34\, W_g / W_{sat}, & W_g / W_{sat} \le 0.5 \\ 0.14 & W_g / W_{sat} > 0.5 \end{cases}.$$

The short-wave radiation is determined from

$$R_{sw} = \tau_{rg}\,\tau_{wv}\,S_0\left(\frac{a^2}{r^2}\right)\cos Z \tag{6.10.10}$$

in which the solar constant is $S_0 = 1353.0\,\mathrm{Wm^{-2}}$, and Earth-Sun distance factor is from

$$\begin{aligned}\frac{a^2}{r^2} = {} & 1.000110 + 0.034221\cos d_0 + 0.001280\sin d_0 + \\ & + 0.000719\cos 2d_0 + 0.000077\sin 2d_0\end{aligned} \tag{6.10.11}$$

where $d_0 = 2\pi m/365$ and m is the day number starting with 0 on Jan. 1 and ending 364 on Dec. 31. The solar zenith angle Z is defined by

$$\cos Z = \sin\phi\,\sin\delta + \cos\phi\,\cos\delta\,\cos\left(h_r\right) \tag{6.10.12}$$

where ϕ is the latitude, δ is the solar declination:

$$\delta = \frac{23.5\pi}{180}\cos\left[2\pi\left(J_d - 173\right)/365\right] \tag{6.10.13}$$

where J_d (= m + 1) is Julian day.

The solar hour angle is defined by:

$$h_r = \frac{15\pi}{180}\left(t_{GMT} - \lambda/15° + E_\tau - 12\right) \tag{6.10.14}$$

where $E_\tau = 0.158\sin\left[\pi\left(J_d + 10\right)/91.25\right] + 0.125\sin\left[\pi J_d/182.5\right]$, (6.10.15)

t_{GMT} is Greenwich Meridian Time, and λ is west longitude (in degrees).

To account for the attenuation by Rayleigh scattering and absorption by permanent gases for solar radiation, the transmission function in (6.10.10) has the form (Atwater and Ball, 1981)

$$\tau_{rg} = 1.021 - 0.084\left[m_{dirf}\left(949\times10^{-8}p + 0.051\right)\right]^{1/2} \tag{6.10.16}$$

where p is the surface pressure (kPa) m_{dirf} is a directional factor that is equivalent to air mass at pressure of 101.3 kPa and follows a formulation given by:

$$m_{dirf} = \frac{35}{\left(1224\cos^2 Z + 1\right)^{1/2}} \tag{6.10.17}$$

The water vapor transmittance in (6.10.10) can be written as

$$\tau_{wv} = 1 - \frac{2.9\mu M_{dirfc}}{\left(1 + 141.5\mu M_{dirfc}\right)^{0.635} + 5.925\mu M_{dirfc}} \tag{6.10.18}$$

where $M_{dirfc} = m_{dirf}$ above any clouds and M_{dirfc} = 5/3 below and within cloud layers. The path length μ at level p is computed from

$$\mu = \frac{1}{g}\int_0^p q_v\left(\frac{p}{101300}\right)\left(\frac{273.16}{T}\right)^{1/2} dp \tag{6.10.19}$$

c) Sensible heat flux

The sensible heat flux

$$H = \rho_a c_p C_{dh} V_a \left(T_s - T_a\right) \tag{6.10.20}$$

where c_p is the specific heat at constant pressure; ρ_a and V_a are, respectively, the air density and wind speed at an atmospheric level; C_{dh} is the exchange coefficient depending upon the thermal stability and roughness.

d) Latent heat flux

The latent heat flux is the sum of the evaporation from the soil surface E_g, transpiration E_{tr}, and evaporation from wet parts of the canopy E_r:

$$LE = L\left(E_g + E_{tr} + E_r\right). \tag{6.10.21}$$

in which L is the latent heat of vaporization and

$$E_g = \left(1 - veg\right)\rho_a C_{dq} V_a \left[h_u q_{vsat}\left(T_s\right) - q_{va}\right] \tag{6.10.22}$$

where the relative humidity at the ground surface is

$$h_u = \begin{cases} 0.5\left[1 - \cos\left(\pi W_g / W_{fl}\right)\right], & W_g < W_{fl} \\ 1, & W_g \geq W_{fl} \end{cases} \tag{6.10.23}$$

with field capacity $W_{fl} = 0.75 W_{sat}$. The saturation mixing ratio q_{vsat} is calculated using Teten's formula given in Eq. (6.3.19).

In (6.10.21) - (6.10.23),

$$E_{tr} = veg\ \rho_a \frac{1 - F_w}{R_a + R_s}\left[q_{vsat}\left(T_s\right) - q_{va}\right] \tag{6.10.24}$$

and

$$E_r = veg\ \rho_a \frac{F_w}{R_a}\left[q_{vsat}\left(T_s\right) - q_{va}\right] \tag{6.10.25}$$

in which the wet fraction of the canopy, F_w, is defined as

$$F_w = \left(\frac{W_r}{W_{rmax}} \right)^{2/3} \tag{6.10.26}$$

and $W_{r\max} = 0.2\ veg\ LAI\ (mm)$. (6.10.27)

Here *LAI* is the leaf area index of vegetation and it depends on the vegetation type. The aerodynamic resistance is parameterized by

$$R_a = \frac{1}{C_{dq} V_a}. \tag{6.10.28}$$

The surface resistance for evapotranspiration is computed as

$$R_s = \frac{R_{smin}}{LAI \quad F_1 F_2 F_3 F_4} \tag{6.10.29}$$

in which

$$F_1 = \frac{f + R_{smin}/R_{smax}}{1 + f} \tag{6.10.30}$$

with $$f = 0.55 \frac{R_G}{R_{GL}} \frac{2}{LAI} \tag{6.10.31}$$

where R_{smax} = 5,000 *s/m*, $R_G = R_{sw}$, and R_{GL} depends on the vegetation type.

$$F_2 = \begin{cases} 1, & W_2 > W_{fl} \\ (W_2 - W_{wilt})/(W_{fl} - W_{wilt}), & W_{wilt} \le W_2 \le W_{fl} \\ 0, & W_2 < W_{wilt} \end{cases} \tag{6.10.32}$$

$$F_3 = \begin{cases} 1 - 0.06\left(q_{vsat}\left(T_a\right) - q_{va}\right), & q_{vsat}\left(T_a\right) - q_{va} \le 12.5\ g/kg \\ 0.25, & otherwise \end{cases} \tag{6.10.32}$$

$$F_4 = 1 - 0.0016\left(298.0 - T_a\right)^2 \tag{6.10.34}$$

e) Soil surface moisture

In (6.10.3), the surface volumetric moisture W_{geq} when gravity balances the capillary force is computed according to

$$\frac{W_{geq}}{W_{sat}} = x - \boldsymbol{a}\, x^{\boldsymbol{p}}\left(1 - x^{8\boldsymbol{p}}\right) \tag{6.10.35}$$

in which

$$x = \frac{W_2}{W_{sat}} . \tag{6.10.36}$$

In (6.10.3), the coefficients are given by

$$C_1 = C_{1sat}\left[\frac{W_{sat}}{W_g}\right]^{\frac{\boldsymbol{b}}{2}+1} \tag{6.10.37}$$

$$C_2 = C_{2ref}\left[\frac{W_2}{W_{sat} - W_2 + W_l}\right] \tag{6.10.38}$$

where W_l is a small numerical value that limits C_2 at saturation. The parameters C_{1sat}, C_{2ref}, b, and p are soil-texture dependent.

Table. 6.2. List of variables used in the soil model.

Name	Description	Coding Name	Where Defined
T_s	Ground surface temperature	tsfc(nx,ny)	ARPS40
T_2	Deep ground temperature	tsoil(nx,ny)	ARPS40
W_g	Soil surface moisture	wetsfc(nx,ny)	ARPS40
W_2	Deep soil moisture	wetdp(nx,ny)	ARPS40
W_r	Canopy moisture	wetcanp(nx,ny)	ARPS40
C_T	Land surface heat capacity	ct	SOILEBM
C_G	Thermal coefficient for bare ground	cg	SOILEBM
C_V	Thermal coefficient for vegetation	cgv	SOILPARAM
$\boldsymbol{b}$	Slope of the retention curve	bslope(13)	SOILPARAM
C_{Gsat}	Thermal coefficient for bare ground at saturation	cgsat	SOILPARAM
veg	Vegetation Fraction	veg14	SOILPARAM
R_n	Net radiation heat flux	rnflx(nx,ny)	SOILEBM
R_{sw}	Downward short wave flux	rsw	RADNET
α	Surface albedo	alf	RADNET
α_s	Soil moisture adjustment of albedo	alfs	RADNET
α_z	Solar zenith angle adjustment of albedo	alfz	RADNET
S_o	Solar constant	solarc	*phycst.inc*
$(a/r)^2$	Squared ratio of average distance of the earth from the sun to its actual distance at any time of the year	a2dr2	SOLRAD
Z	Solar zenith angle	zenith (nx,ny)	SOLRAD
ϕ	Latitude at scalar points	latscl(nx,ny)	SOILEBM
δ	Solar declination	sdeclin	SOLRAD
J_d	Julian day	jday	INITPARA
hr	Solar hour angle	shrangl	SOLRAD
e_τ	Equation of time	etau	SOLRAD
τ	Length of the day	tau	SOILEBM
τ_{rg}	Transmittance after Rayleigh scattering and absorption by gases	trrg	RADNET
τ_{wv}	Water vapor transmittance	trwv	RADNET
m_{dirf}	Directional factor of Rayleigh scattering and absorption	dirf	SOILEBM
M_{dirfc}	Directional factor of Rayleigh scattering and absorption by cloud	dirfc	SOILPARAM
μ	Precipitation path length	prcpln(nx,ny)	SOILEBM
ε_g	Emissivity of the ground	emissa	*phycst.inc*
ε_a	Emissivity of the atmosphere	emissg	*phycst.inc*
σ	Stefen-Boltzmann constant	sbcst	*phycst.inc*
H	Sensible heat flux	shflx(nx,ny)	SOILEBM
ρ_a	Air density at anemometer level	rhoa(nx,ny)	SOILEBM
V_a	Wind speed at anemometer level	windsp(nx,ny)	SOILEBM
T_a	Air temperature at anemometer level	tair(nx,ny)	SOILEBM
q_{va}	Mixing ratio at anemometer level	qvair(nx,ny)	SOILEBM
$q_{vsat}\ (T_S)$	Surface saturated mixing ratio	qvsatts	EVAPFLX
$q_{vsat}\ (T_a)$	Saturated mixing ratio at anemometer level	qvsata	EVAPFLX
C_1	Coefficient of the net precipitation	c1wg	SOILEBM

Table. 6.2. Continued ...

Name	Description	Coding Name	Where Defined
C_2	Coefficient of the perturbated near surface moisture content	c2wg	SOILEBM
C_{1sat}	Value of C_1 at saturation	c1sat	SOILEBM
C_{2ref}	Value of C_2 at $W_2 = 0.5\ W_{sat}$	c2ref	SOILEBM
W_{geq}	Surface moisture when gravity and the capillary forces are balanced	wgeq	SOILEBM
a	Coefficient in W_{geq} formula	awgeq(13)	SOILPARAM
p	Exponent in W_{geq} formula	pwgeq(13)	SOILPARAM
h_u	Relative humidity at ground surface	rhgs	SOILEBM
W_{fl}	Field capacity of soil moisture	wfc(13)	SOILPARAM
h_v	Halstead coefficient	hv	SOILEBM
δ	Fraction of foliage covered by intercepted water	delta	EVAPFLX
E_r	Direct evaporation from the fraction δ of foliage	evaprr(nx,ny)	EVAPFLX
E_{tr}	Transpiration of the dry portion (1-δ) of leaves	evaprtr(nx,ny)	EVAPFLX
E_v	Evapotranspiration from vegetation	evaprv(nx,ny)	EVAPFLX
E_g	Evaporation from ground	evaprg(nx,ny)	EVAPFLX
P	Precipitation rate	precip(nx,ny)	SOILEBM
R_a	Aerodynamic resistance	(see rstcoef)	EVAPFLX
R_s	Surface resistance	(see rstcoef)	EVAPFLX
W_{max}	Maximum value of vegetation moisture W_r	wrmax	SOILEBM
F_1	Fractional conductance of photosynthetically active radiation	(see rstcoef)	EVAPFLX
F_2	Fractional conductance of water stress	(see rstcoef)	EVAPFLX
F_3	Fractional conductance of atmospheric vapor pressure	f34(nx,ny)	SOILEBM
F_4	Fractional conductance of air temperature	f34(nx,ny)	SOILEBM
LAI	Leaf Area Index	lai(nx,ny)	SOILEBM
R_{smin}	Minimum of surface resistance	rsmin(14)	SOILEBM
R_{smax}	Maximum of surface resistance	rsmax	SOILEBM
R_{gl}	Species-dependent threshold value of incoming radiation	rgl(14)	SOILPARAM
W_{wilt}	Wilting point of soil moisture	wwlt(13)	SOILPARAM

6.11. Cumulus Parameterization Schemes

A modified Kuo scheme has been implemented in ARPS 4.0. We plan to add an option of another cumulus scheme (*e.g.*, Kain and Fritsch, 1993) in the near future.

6.11.1. Modified Kuo scheme

The Kuo scheme (Kuo, 1965, 1974) is one of the earliest and most enduringly popular schemes for cumulus parameterization. A critique of this scheme can be found in Raymond and Emanuel (1993). In this scheme, the amount of convection is determined by the vertically integrated moisture convergence. The feedback to the large scale (the vertical distribution of heating and moistening) is represented by the terms S_θ (neglecting the radiative heating) and S_{q_v} in (6.2.25) and (6.2.27), respectively. The user is required to specify: (i) *confrq*, a frequency of the computing cumulus scheme; and (ii) *wcldbs*, a critical threshold value of the vertical velocity at cloud base.

In the Kuo scheme, the vertical structure of cumulus heating is assumed to be in the form of a relaxation toward a moist adiabat θ_a, *i.e.*,

$$S_\theta \equiv \frac{\rho^*(\theta_a - \theta)}{\tau} \tag{6.11.1}$$

where τ is a relaxation time, and it can be related to the fraction of the available moisture supply (1-*b*)M_t that participates in the heating of an atmospheric column:

$$\tau = \frac{1}{L\,(1-b)\,M_t} \int_0^{Z_t} \rho^* \pi\ (\theta_a - \theta)\, dz \tag{6.11.2}$$

in which π ($\equiv c_p T/\theta$) is the Exner function, L is the latent heat of evaporation, (1-*b*) is the precipitation efficiency that is inversely proportional to wind shear (Fritsch and Chappell, 1980), and M_t, the available moisture supply, is given by

$$M_t = -\int_0^{Z_t} Wc^* \frac{\partial q}{\partial z} dz + \mathrm{E} \tag{6.11.3}$$

where E is the surface moisture flux as defined in Eq. (6.10.21).

The rate of precipitation (per unit area) due to cumulus convection is given by

$$P_{cum} = (1-b)\, M_t \tag{6.11.4}$$

In ARPS code, the procedure of computing S_θ at each grid point can be summarized as follows:

1. Compute M_t according to Eq. (6.11.3), and check whether M_t is greater than a critical threshold value.
2. Compute moist adiabat θ_a based on model sounding.
3. Determine cloud top and cloud base from model sounding, and check whether cloud depth is deep enough and cloud top is higher than 500mb level.
4. Check whether the vertical velocity at cloud base is greater than *wcldbs*, a critical threshold value specified by the user.
5. Check the model sounding for convective instability to see if convection is allowed.
6. If conditions in steps 3 to 5 are all met, then compute S_θ according to Eqs. (6.11.1) and (6.11.2).